Cell

Resource

Temporally multiplexed imaging of dynamic signaling networks in living cells

Graphical abstract

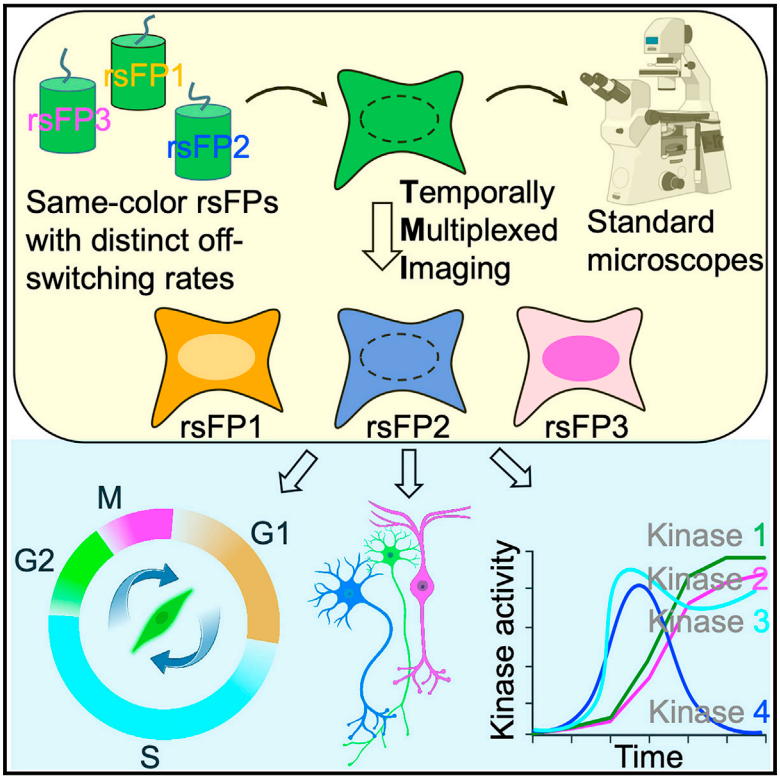

Highlights

- TMI computationally separates signals from fluorophores with different switching kinetics
- TMI enables imaging of many signals at once, in living cells, using standard microscopes
- TMI can be used to image cytoskeletal structures and organelles in living cells
- TMI can report gene expression, kinase activity, protein movement, and other signals

Authors

Yong Qian, Orhan T. Celiker, Zeguan Wang, Burcu Guner-Ataman, Edward S. Boyden

Correspondence

edboyden@mit.edu

In brief

In temporally multiplexed imaging (TMI), many dynamic signals can be imaged in the same living cell, using a standard microscope, by associating different cellular signals with genetically encoded fluorophores with distinct clocklike properties.

Qian et al., 2023, Cell *186*, 1–17
December 7, 2023 © 2023 The Authors. Published by Elsevier Inc.
https://doi.org/10.1016/j.cell.2023.11.010

CellPress

Please cite this article in press as: Qian et al., Temporally multiplexed imaging of dynamic signaling networks in living cells, Cell (2023), https://doi.org/10.1016/j.cell.2023.11.010

Cell

CellPress
OPEN ACCESS

Resource

Temporally multiplexed imaging of dynamic signaling networks in living cells

Yong Qian,[1] Orhan T. Celiker,[1,2] Zeguan Wang,[1,3] Burcu Guner-Ataman,[1] and Edward S. Boyden[1,3,4,5,6,7,8,9,*]
[1]McGovern Institute for Brain Research, Massachusetts Institute of Technology (MIT), Cambridge, MA 01239, USA
[2]Department of Electrical Engineering and Computer Science, MIT, Cambridge, MA 01239, USA
[3]Department of Media Arts and Sciences, MIT, Cambridge, MA 01239, USA
[4]Department of Brain and Cognitive Sciences, MIT, Cambridge, MA 01239, USA
[5]Department of Biological Engineering, MIT, Cambridge, MA 01239, USA
[6]Koch Institute, MIT, Cambridge, MA 01239, USA
[7]Howard Hughes Medical Institute, Cambridge, MA 01239, USA
[8]Center for Neurobiological Engineering and K. Lisa Yang Center for Bionics at MIT, Cambridge, MA 01239, USA
[9]Lead contact
*Correspondence: edboyden@mit.edu
https://doi.org/10.1016/j.cell.2023.11.010

SUMMARY

Molecular signals interact in networks to mediate biological processes. To analyze these networks, it would be useful to image many signals at once, in the same living cell, using standard microscopes and genetically encoded fluorescent reporters. Here, we report temporally multiplexed imaging (TMI), which uses genetically encoded fluorescent proteins with different clocklike properties—such as reversibly photoswitchable fluorescent proteins with different switching kinetics—to represent different cellular signals. We linearly decompose a brief (few-second-long) trace of the fluorescence fluctuations, at each point in a cell, into a weighted sum of the traces exhibited by each fluorophore expressed in the cell. The weights then represent the signal amplitudes. We use TMI to analyze relationships between different kinase activities in individual cells, as well as between different cell-cycle signals, pointing toward broad utility throughout biology in the analysis of signal transduction cascades in living systems.

INTRODUCTION

Microscopy of living cells expressing fully genetically encoded fluorescent reporters of molecular signals is important for measuring the dynamics of these signals in relation to one another and to cellular states, subcellular locations, and emergent functions. Multiplexed fluorescence imaging enables the ability to see more than one signal at a time, in an individual living cell, so that relationships between the signals can be discovered.[1–4] Without this ability, it is hard to determine the relationships between different signals, key to analyzing how they interact to yield cellular computations, and how such biological processes go wrong in disease states. As a simple example, suppose when signal A is high in a given cell, signal B goes low, and when signal A is low in a given cell, signal B goes high—perhaps because A suppresses B. Imaging of A and B in separate cells would miss out on this relationship; only by measuring them in the same cell will the relationship be easily seen. Of course, in most real biological signaling networks, many more than two signals will interact to generate a given biological computation. For example, protein kinase A (PKA) interacts with multiple mitogen-activated protein kinases (MAPKs), such as extracellular signal-regulated kinase (ERK), c-Jun NH_2-terminal kinase (JNK), and P38 kinase, when cells are stimulated with various inputs. But the relationships are context dependent: PKA might drive, suppress, or have no effect on a given kinase, depending on the details of the stimulus received, pointing to ways in which network topology could be regulated by cellular input.[5–7]

Traditionally, on the conventional microscopes commonly used in biology, multiplexed fluorescence imaging has relied on spectral differences between the fluorophores used to report different signals, which limits the number of signals observable to just 2–3, and occasionally 4.[8,9] Techniques utilizing non-standard microscope hardware, including multiplexed fluorescence lifetime imaging microscopy (FLIM),[10–12] spectral deconvolution,[3,13,14] and Raman spectroscopy,[15] have expanded the number of observable signals to >5. However, although pioneering, these techniques rely on specific microscope hardware, including optic and/or electronic hardware that can be expensive and technically demanding, in addition to being inaccessible to biologists using only conventional microscopes. Moreover, these techniques may require the use of non-genetically encoded chemicals (e.g., synthetic dyes for FLIM and spectral deconvolution and phenyl-capped polyynes for Raman microscopy) to be able to reach their maximum multiplexing capacity, which raises the complexity of live-cell imaging, in

This is an open access article under the CC BY license (http://creativecommons.org/licenses/by/4.0/).

Please cite this article in press as: Qian et al., Temporally multiplexed imaging of dynamic signaling networks in living cells, Cell (2023), https://doi.org/10.1016/j.cell.2023.11.010

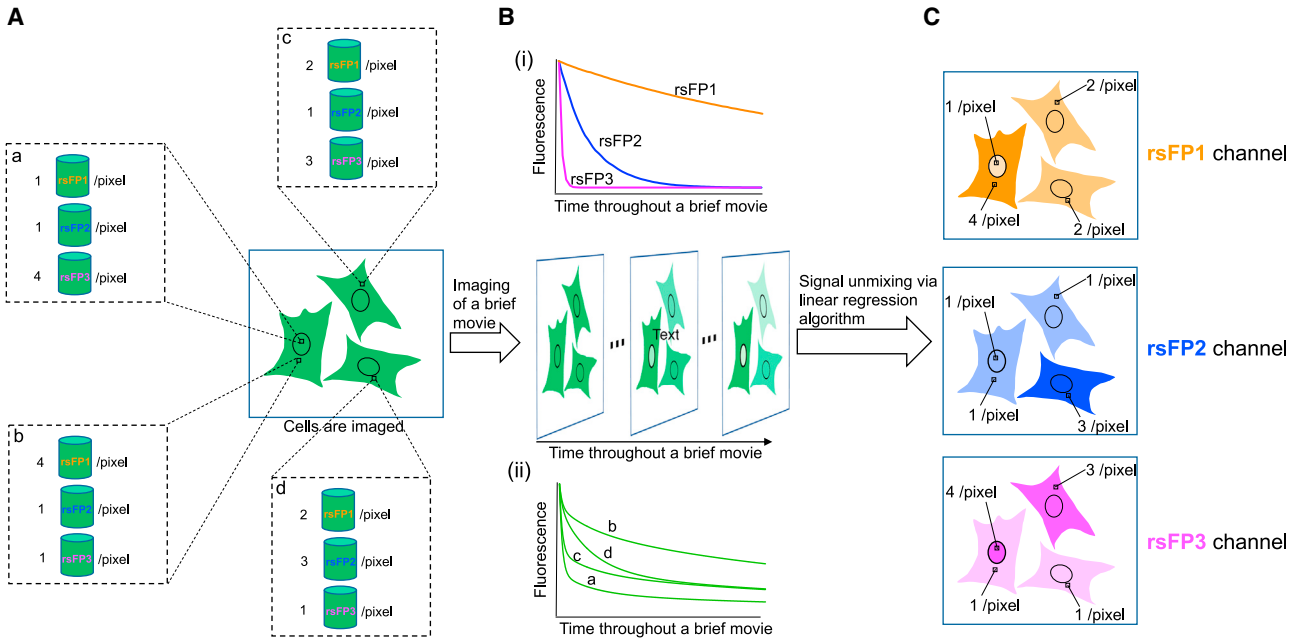

Figure 1. Concept of temporally multiplexed imaging, implemented using reversibly photoswitchable fluorescent proteins

(A) Multiple rsFPs (denoted 1 through 3), even of the same color (text colors do not reflect fluorophore color but are simply for reference later in the figure), are expressed in cells. A signal is indicated by the amount of a given fluorophore in a given pixel in an image of a cell, "Aa" through "Ad" represent different pixels exhibiting the indicated numbers of rsFP1, rsFP2, and rsFP3 molecules ("Aa" is in the nucleus; "Ab," "Ac," and "Ad" are in the cytosol). These rsFPs are spectrally indistinguishable by conventional microscopes.

(B) Despite their spectral similarity, these rsFPs behave differently over time during continuous imaging for a brief period (e.g., a few seconds) (Bi). The fluorescence trace of each pixel acquired during a brief movie, obtained during an experiment (Bii), is a linear combination of all the rsFP reference traces (Bi), each weighted by the number of fluorophores of that kind present at that pixel.

(C) The fluorescence intensity of each rsFP at each pixel is obtained via standard linear unmixing of the fluorescence trace acquired during the brief movie in (B). The resultant images can then be pseudo-colored for visualization, by giving each rsFP a different digital color in software (here, orange, blue, and pink for rsFP1, rsFP2, and rsFP3, respectively).

which genetically encoded reporters have played a dominant role since the discovery of fluorescent proteins (FPs).[16,17] Thus, a strategy for highly multiplexed live-cell imaging would ideally be cost-effective and easy to implement, and it would require only ordinary microscopes and use only fully genetically encoded fluorescent reporters.

We recently developed a multiplexing strategy that uses self-assembling peptides to cluster existing genetically encoded, dynamic fluorescent reporters at random but stable points throughout living cells, so the different signals can be imaged separately by a conventional microscope.[1] Such a spatially multiplexed imaging (SMI) strategy can measure cellular signals present at the location of each cluster, with greater multiplexing capacity than feasible with spectral multiplexing. However, given the spatial nature of its encoding of reporter identity, SMI cannot be used to visualize the organization of proteins in living cells or organelles or to visualize protein movement in response to a stimulus. SMI also cannot easily measure changes indicated by the amount of protein present, such as cellular gene expression, or local protein translation. Nevertheless, the use of space as a resource to facilitate imaging in SMI—a theme used in other imaging developments such as expansion microscopy[18]—raises the question of whether other unconventional resources such as time could also be used to enhance the number of signals simultaneously observable in a living cell.

We here report that by using fluorophores that exhibit different clocklike properties, to indicate different cellular signals, a brief movie (taken over a period of a few seconds) that records the temporal information of the fluorescence at each pixel can be inverted using standard unmixing linear algebra to yield the individual signal amplitudes at that pixel. The signal amplitudes at each pixel are simply the coefficients that are multiplied by each fluorophore's standard temporal fluctuation trace, which when summed up in weighted form, make up the recorded trace obtained at that pixel (Figure 1). We here use reversibly photoswitchable FPs (rsFPs) with different off-switching rates to achieve the clocklike effect, although in principle any temporally fluctuating signal might be adaptable to this concept. We show that temporally multiplexed imaging (TMI) can support the imaging of more signals at once than are feasible with traditional spectral multiplexing on a conventional microscope using fully genetically encoded reagents, revealing relationships between cell-cycle proteins as well as between different kinase activities. TMI requires no hardware beyond a standard fluorescence microscope, commonly available to biologists, and uses fully genetically encoded fluorescent reporters that fit into standard biology workflows.

Please cite this article in press as: Qian et al., Temporally multiplexed imaging of dynamic signaling networks in living cells, Cell (2023), https://doi.org/10.1016/j.cell.2023.11.010

CellPress
OPEN ACCESS

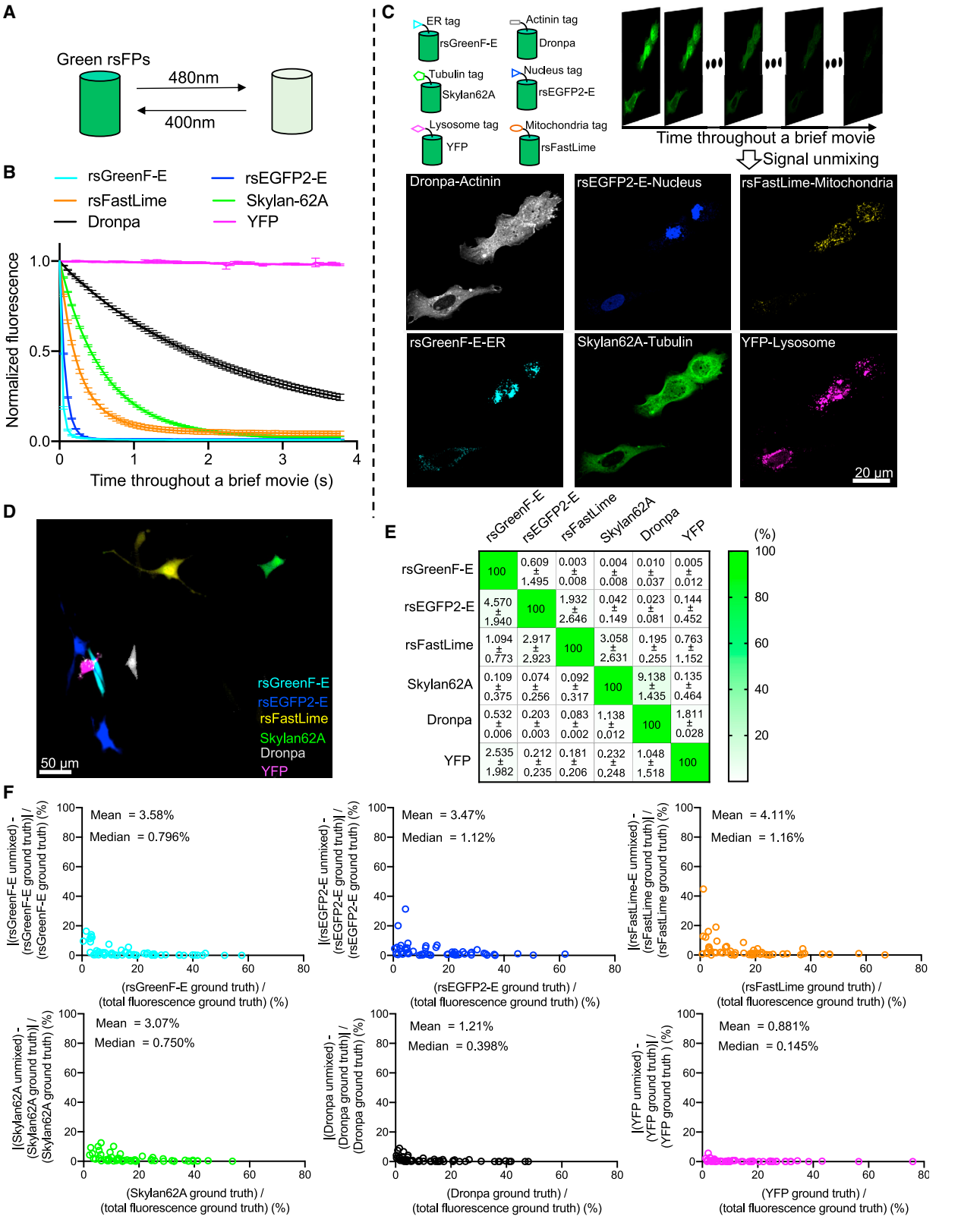

(legend on next page)

Please cite this article in press as: Qian et al., Temporally multiplexed imaging of dynamic signaling networks in living cells, Cell (2023), https://doi.org/10.1016/j.cell.2023.11.010

RESULTS

TMI concept

In our initial implementation of TMI, multiple rsFPs, even those of the same color but exhibiting different clocklike behaviors (i.e., different off-switching rates during continuous illumination), are expressed in the same cell (Figure 1A). Since each fluorophore behaves differently over time (Figure 1Bi)—in the case of rsFPs, they display different exponential decay curves (note well, this is not photobleaching,[19] as the process is fully reversible by illumination with a second color of light)—pixels that contain different amounts of each fluorophore will exhibit different trajectories of fluorescence decay over the timescale of a brief (few-second-long) movie (Figure 1Bii). (Note also that this is not fluorescence lifetime, which is too fast [nanoseconds] to be measured on ordinary fluorescence microscopes; TMI movie acquisition only requires conventional cameras.) By computationally unmixing the fluorescence trace at each pixel (Figure 1Bii) into a linear combination of the traces exhibited by each fluorophore alone (Figure 1Bi; these reference traces are derived in a separate experiment, with just one fluorophore present, under the same imaging conditions), one can reconstruct the amplitude of each signal at that pixel—it is simply the weight associated with that fluorophore's reference trace, when the sum is unmixed (Figure 1C).

TMI of six green FPs, and imaging of subcellular structure

To validate this concept, we first explored green rsFPs, such as those whose fluorescence can be switched off by blue light and switched on by purple light (Figure 2A). We chose a set of green rsFPs with distinct off-switching kinetics (Figure 2B). Dronpa,[20] rsFastLime,[21] and rsGreenF-Enhancer (rsGreenF-E)[22] exhibited highly different off-switching kinetics (Figure 2B). Skylan-NS[23] had kinetics similar to rsFastLime (Figure S1A), so we performed directed evolution (Figure S1B) to create a variant with kinetics between those of rsFastLime and Dronpa, which we named Skylan62A (Figure S1C). rsEGFP2-Enhancer (rsEGFP2-E)[22,24] had off-switching kinetics between those of rsGreenF-E and rsFastLime (Figure S1D). A non-switching FP, yellow fluorescent protein (YFP),[25] served as a 6th distinguishable candidate (Figure 2B). Each FP exhibited off-switching time courses independent of expression level, indicating robustness of the clocklike property in indicating signal amplitude (Figures S1E–S1J). Off-switching traces were well-fit by single-component exponential decays (Figures S1K and S1L).

We expressed these FPs in cultured cells, each fused to a distinct, well-validated, subcellular targeting sequence. One potential concern is that expressing many genes at once could cause the cell to express abnormally high levels of exogenous protein. However, cells co-expressing all six FPs had overall expression levels of exogenous protein comparable to those of cells expressing only one FP (Figure S1M). We fixed the cells (for subsequent immunostaining-based validation) and acquired brief (70-frame) movies over 3.8 s on a confocal microscope. We unmixed the brief movies using the reference traces (Figure 2B; acquired under identical conditions), using standard unmixing linear algebra (see STAR Methods), and found that indeed we could recapitulate known cellular morphologies (Figure 2C). Summing reference traces weighted by the signal amplitudes reconstituted the original traces (Figure S2A). We compared TMI-derived images with those obtained by antibody staining against a FLAG tag fused to each of the six FPs in turn and found no difference in rsFP-antibody correlation when rsFPs were expressed individually (the ground truth) vs. when they were all expressed together (Figures S2B and S2C). Thus, TMI crosstalk between different rsFPs is minimal.

As a second measure of TMI crosstalk, we expressed rsFPs in individual NIH/3T3 cells, with each cell expressing only one FP (a ground truth), and measured the crosstalk of each FP to the other five (Figure 2D), finding crosstalk to be in the few percent range and often lower (Figure 2E). As a third measure of TMI crosstalk, we simulated a 70-frame video starting with an image of NIH/3T3 cells, with each pixel of the video exhibiting a simulated linear combination of the six fluorophores' exponential decays, with added noise (see STAR Methods for details). Unmixing the resulting brief movie would then reconstruct the single-fluorophore images (Figure S2D), which, being simulated, serve as a ground truth. We obtained near-perfect Pearson's correlation values between thus-unmixed images and source ground-truth images (Figure S2D). Most individual cells (Figure 2F) deviated from the ground truth by a few percent or less (although for extremely dim cells, the error could of course be greater). Thus, through several independent validations, we found that linear unmixing of brief (few-second-long) movies of cells containing mixtures of rsFPs yielded accurate reconstructions of signals. We note that reconstruction proceeded well regardless of lens magnification (40× objective lenses were used for validation 1, and 20× objective lenses for validations 2 and 3).

TMI of four red FPs, and red FP-based single-color brainbow

Off-switching red rsFPs can be switched to a dim state with orange light and can resume fluorescing under blue or purple light (Figure 3A). rsTagRFP[26] and rsFusionRed1[27] exhibited switching rates appropriate for TMI (Figure 3B). We engineered rScarlet

Figure 2. Temporally multiplexed imaging of green fluorescent proteins

(A) Green rsFPs can be switched "off" by ~480 nm light and switched "on" by ~400 nm light.

(B) Reference traces (as in Figure 1Bi, top) of green FPs in U2OS cells under illumination at 488 nm at 40 mW/mm^2. Mean ± standard deviation (SD), n = 10–15 cells each (from 3 brief movies from 1 cell culture).

(C) Organelle- or cytoskeletally targeted FPs in U2OS cells, imaged via TMI, using the reference traces in (B).

(D) Representative merged image (out of 15 merged images taken from 2 cell cultures) of live NIH/3T3 cells expressing green FPs individually (not fused to targeting tags; reference traces calibrated in living NIH/3T3 cells) assembled from six raw images unmixed from the source brief movie.

(E) FP-FP crosstalk, calculated from the linear decomposition coefficients extracted from 15 merged images from 2 cultures experimented upon as in (D) and expressed as percentage of true FP brightness. Mean ± SD; color represents mean.

(F) Accuracy of linear decomposition of TMI brief movies into individual FP images, simulated using reference traces of (B). Each data point represents one cell. See also Figure S1 and S2.

Please cite this article in press as: Qian et al., Temporally multiplexed imaging of dynamic signaling networks in living cells, Cell (2023), https://doi.org/10.1016/j.cell.2023.11.010

CellPress
OPEN ACCESS

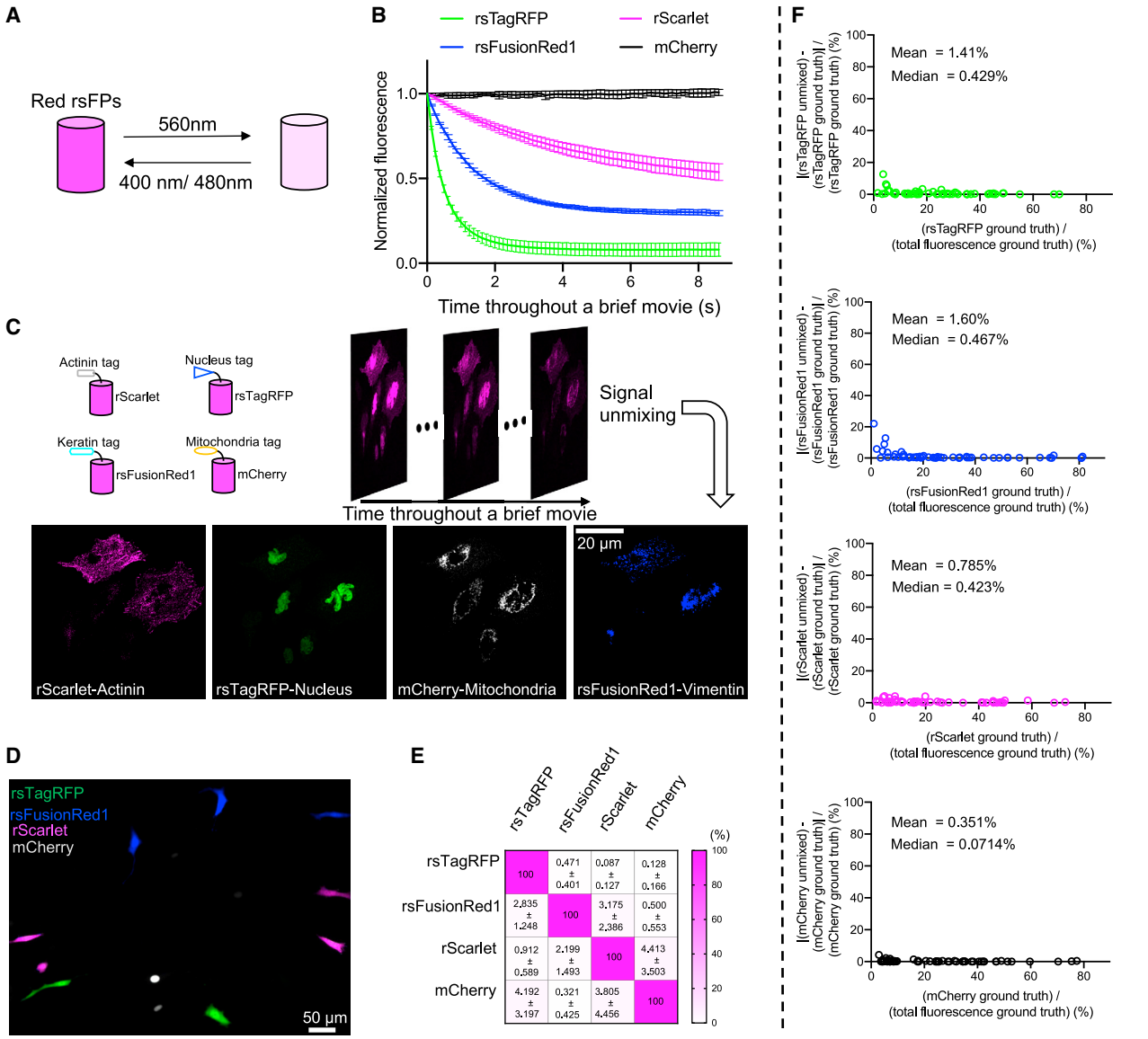

(legend on next page)

Please cite this article in press as: Qian et al., Temporally multiplexed imaging of dynamic signaling networks in living cells, Cell (2023), https://doi.org/10.1016/j.cell.2023.11.010

from mScarlet[28–30] (Figure S3A) to serve as a third red TMI fluorophore (Figures 3B, S3B, and S3C). mCherry,[31] which is non-switching, served as a fourth red fluorophore. Red rsFPs exhibited off-switching traces that were independent of expression level (Figures S3D–S3G) and well-fit by single-component exponential decays (Figures S3H and S3I). We co-expressed the four red FPs, with each FP fused to a different subcellular targeting sequence (again, overall expression of the four exogenous FPs was similar in amount to that of a single exogenous FP; Figure S3K); we fixed the cells and acquired brief (70-frame) movies over 8.6 s on a confocal microscope. Each unmixed image showed the expected subcellular labeling (Figure 3C), with minimal crosstalk when validated with antibody staining against epitope-tagged indicators (Figure S3J). When the FPs were expressed in NIH/3T3 cells individually, the crosstalk between each pair of FPs was in the few percent range or lower (Figures 3D and 3E). Repeating the simulation described above with red rsFPs provided independent confirmation that they could support extremely low crosstalk (Figures 3F and S3L). Thus, as with green rsFPs, red rsFPs could support high-quality and robust TMI imaging.

Brainbow, the combinatorial expression of FPs for cell identification,[32] requires multispectral imaging, limiting the spectrum usable for optical imaging and perturbation of dynamic signals. A TMI form of brainbow could free up spectrum for live imaging of cellular processes. We transiently expressed rsTagRFP, rsFusionRed1, and rScarlet in the nervous system of zebrafish larvae in a mosaic fashion.[33,34] By imaging all three fluorophores over 8.6 s of brief movie recording, in the red channel, and then unmixing the fluorophores, we obtained brainbow-like images in living zebrafish brains via TMI (Figure 3G; with additional figures including those of neurites in Figure S3M). In contrast to standard brainbow, TMI-based brainbow only requires one color channel and thus could free up spectrum for purposes such as imaging Ca^{2+} or neurotransmitters or for optogenetics.

Imaging of multiple dynamic signals with TMI in living cells

We next explored whether TMI could help with imaging dynamics in living cells. Fluorescent, ubiquitination-based cell-cycle indicator 4 (FUCCI4) is an indicator system that reports all four cell-cycle phases using cell-cycle-regulated proteins fused to spectrally distinct FPs.[35] A TMI version of FUCCI4 could free up spectrum for imaging of other cell-cycle-related signals. We replaced the FPs in the original FUCCI4 with four TMI FPs (Figure 4A). Specifically, Dronpa, YFP, rsGreenF-E, and Skylan62A were fused to a specific fragment of Cdc10-dependent transcript 1 ($Cdt_{130–120}$), a fragment of human stem-loop binding protein ($SLBP_{18–126}$), $Geminin_{1–110}$, and histone H1.0, respectively. Analogous to the original FUCCI4, the G1-S transition is reported by the emergence of rsGreenF-E fluorescence while YFP fluorescence persists, and the S-G2 transition is marked by the loss of YFP amid stable rsGreenF-E fluorescence. Chromosome condensation, as reported by Skylan62A, indicates the M phase; loss of rsGreenF-E fluorescence and the appearance of Dronpa and YFP fluorescence mean the beginning of G1. We imaged NIH/3T3 cells using TMI FUCCI4 and were able to identify cell-cycle transitions just as with original FUCCI4 (Figures 4B and 4C; with additional examples in Figure S4A). TMI versions of other cell-cycle reporter systems, e.g., FUCCI(C/A),[36] may also be of use.

We next explored whether TMI could help with the imaging of protein movement or of signals indicated by protein movement. Kinase translocation reporters (KTRs) report kinase activity increases by translocating from the nucleus to the cytoplasm[37] (Figure 4D). We replaced the FPs in the original KTRs for JNK, ERK, and P38 with rsGreenF-E, rsFastLime, and Dronpa, respectively. Together with PKA KTR-Clover (Clover being a non-photoswitching FP), we performed TMI with four kinase sensors simultaneously (as with FPs, overall expression of four KTRs resulted in an overall exogenous protein expression amount similar to that of a single KTR alone; Figure S4B). TMI of four kinase sensors required us to take many brief movies one after the other (i.e., every 2 min for 1 h), but the protocol used did not result in an increase in reactive oxygen species (ROS) (Figure S4C; our cell-cycle imaging protocol did not induce such stress either, Figure S4D; for comparison, blue light excitation as used for calcium imaging[38–40] did increase ROS, Figure S4C). Our TMI imaging protocol also did not change JNK, ERK, P38, or PKA activity, as reported by their KTR reporters (Figure S4E).

We imaged NIH/3T3 cells expressing the aforementioned KTRs and delivered mouse basic fibroblast growth factor 2 (bFGF2, 20 ng/mL), which is known to drive kinases such as ERK, JNK, P38, and PKA.[41–44] The response, averaged across all cells, was a fast onset of ERK activity (Figure 4E–4G; with all raw traces in Figures S5A and S5B), followed by slower but steady increases in JNK, PKA, and P38 activities. We wondered if by examining the relationship between the activity of one kinase and the activity of another kinase, across individual cells, patterns might emerge, which might lead to new hypotheses about how the different kinase activities relate to one another. Such hypotheses, if this paper were a full scientific study rather

Figure 3. Temporally multiplexed imaging of red FPs

(A) Red rsFPs switch off with ~560 nm light and switch on with ~480 or ~400 nm light.

(B) Reference traces of red FPs in U2OS cells. 10–15 cells each, from 1 culture; mean ± SD; 561 nm at 50 mW/mm^2.

(C) Organelle- or cytoskeletally targeted red FPs in U2OS cells, imaged via TMI, using the reference traces in (B).

(D) Representative merged image (out of six merged images taken from two cell cultures) of live NIH/3T3 cells with expression of four red FPs individually (not fused to targeting tags) from four raw images unmixed from the source brief movie.

(E) FP-FP crosstalk, calculated from the linear decomposition coefficients extracted from six merged images from two cultures experimented upon as in (D) and expressed as a percentage of the true FP brightness for a given cell. Values are shown as mean ± SD; color represents the mean.

(F) Accuracy of TMI of four red FPs, using the same simulation and analysis methods as in Figure 2F.

(G) Single-color "brainbow" in larval zebrafish brain. Middle, representative conventional fluorescence image (out of 20 images taken from 3 animals) of zebrafish larval hindbrain (dorsal view); right, brainbow-like image obtained via TMI, showing the same area as in the middle panel.

See also Figure S3.

Please cite this article in press as: Qian et al., Temporally multiplexed imaging of dynamic signaling networks in living cells, Cell (2023), https://doi.org/10.1016/j.cell.2023.11.010

CellPress
OPEN ACCESS

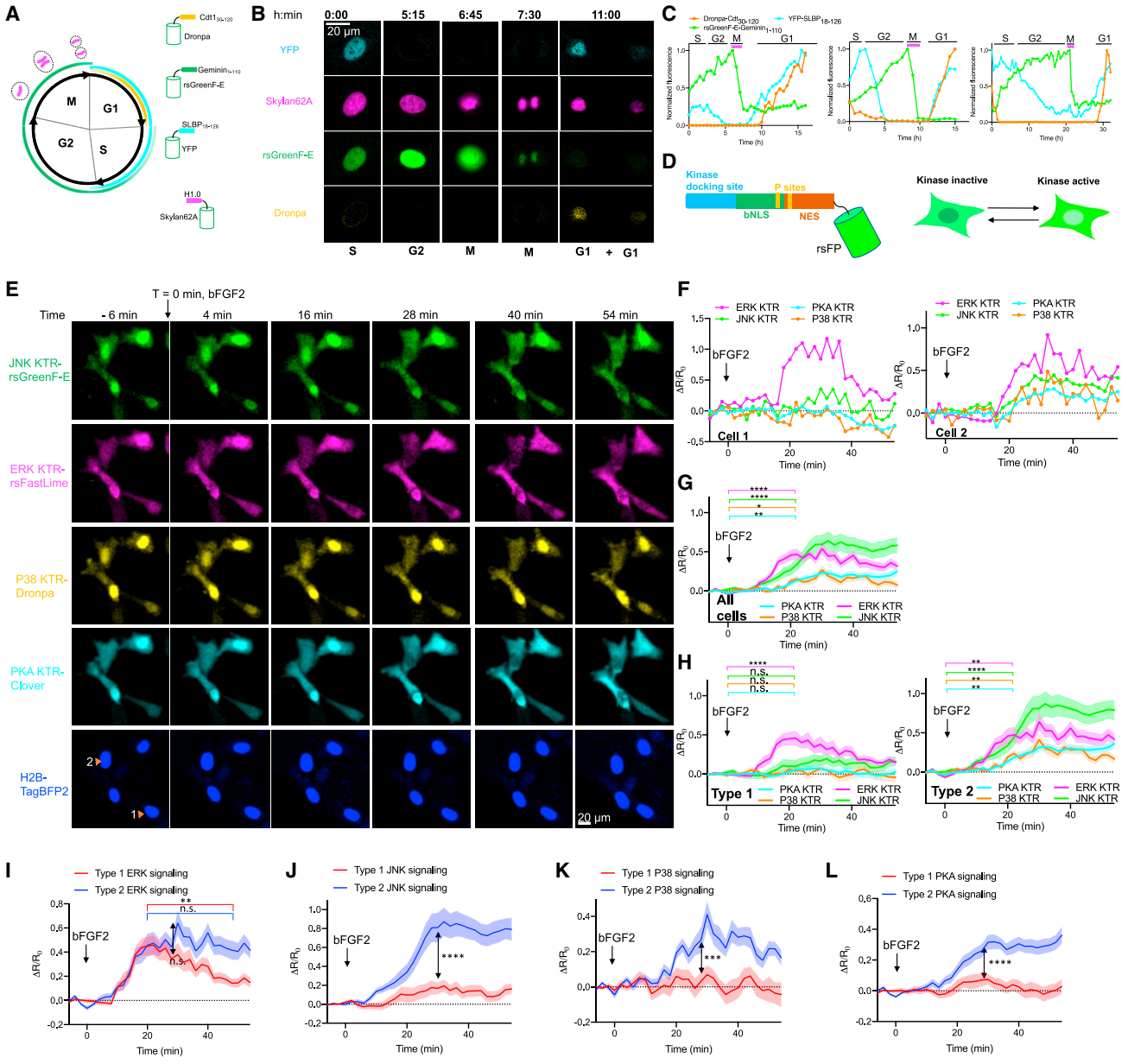

Figure 4. Temporally multiplexed imaging allows for simultaneous observation of many biological signals at once in a single living cell

(A) Diagram of TMI-based FUCCI4.

(B) Tracking of cell-cycle phase in NIH/3T3 cells via time-lapse imaging (i.e., taking brief movies at different points in time, each of which yields a distinct set of images) using TMI-based FUCCI4. A mother cell dividing into two daughter cells was captured during an 11-h imaging session. Two plasmids were used (and in C): CMV::rsGreenF-E-Geminin$_{1–110}$-IRES-Dronpa-Cdt$_{30–120}$ and CMV::YFP-SLBP$_{18–126}$-IRES-H1.0-Skylan62A.

(C) Fluorescence traces (normalized to maximum) of TMI-based FUCCI4 (as in A and B) for three cells during division, tracing one arbitrary daughter cell from each mother cell after M phase. Magenta bars, time of chromosome condensation.

(D) Diagram of TMI-based KTRs.

(E) NIH/3T3 cells expressing TMI-based KTRs and H2B-TagBFP2 imaged before and after delivery of 20 ng/mL bFGF2. Four representative cells (out of 30 cells from 2 cell cultures) are shown. Two plasmids were used: GAG::JNKKTR-rsGreenF-E-P2A-ERKKTR-rsFastLime-IRES-PKAKTR-Clover-P2A-P38KTR-Dropna and CMV::H2B-TagBFP2.

(F) Activity traces of four kinases from two representative cells of (E) (indicated by orange triangles). Left, a representative type 1 cell; right, a representative type 2 cell—as defined in the text. R, ratio of cytoplasmic intensity to nuclear intensity; R_0 is the average value from t = −6 to t = −4 min.

(G and H) Averaged traces of four kinase activities recorded from all NIH/3T3 cells (G, n = 30 cells from two culture batches (see Figures S5A and S5B for traces of individual cells)), or just type 1 (H, left, n = 12 cells) or type 2 cells (H, right, n = 18 cells). Mean ± standard error of the mean (SEM); Wilcoxon rank-sum tests between the averaged values from t = −6 to t = 0 min and the averaged values from t = 18 to t = 24 min. Full statistics for this and other figures, Table S3.

(legend continued on next page)

Please cite this article in press as: Qian et al., Temporally multiplexed imaging of dynamic signaling networks in living cells, Cell (2023), https://doi.org/10.1016/j.cell.2023.11.010

than a technology paper, could be tested by causal intervention, pharmacology, and the full gamut of techniques available to biological investigators, potentially revealing how the kinases interact, perhaps directly or through intermediates. Here, we simply explore the kinds of patterns that TMI can reveal, and we do not intend for these observations to be taken as a complete scientific story but rather as examples of the kind of hypotheses that TMI can yield. We noticed that cells appeared to fall into two categories, based upon their ERK kinase responses. "Type 1" cells (and again, we do not intend for these classifications to be considered as conclusive but instead as simply illustrative of the kinds of patterns TMI can reveal) we defined as having a decline in ERK activity after peak ERK activity was reached (to be precise, $((\Delta R/R_0)\text{max} - (\Delta R/R_0)\text{tail})/(\Delta R/R_0)\text{max} \geq 40\%$, where $(\Delta R/R_0)$tail is defined to be the average of the values taken at the last three time points). In this type of cell, JNK, PKA, and P38 exhibited minimal to no activity throughout the entire experiment (Figures 4F, 4H–4L, and S5A). In contrast, "type 2" cells, defined as those that exhibited sustained ERK activity after peak ERK activity was reached $(((\Delta R/R_0)\text{max} - (\Delta R/R_0)\text{tail})/(\Delta R/R_0)\text{max} < 40\%)$ exhibited elevated JNK, PKA, and P38 activity in response to bFGF2 (Figures 4F, 4H–4L, and S5B). These results suggest that two configurations of this signaling pathway might exist in NIH/3T3 cells in response to bFGF2 stimulation, with ERK activity potentially reinforcing the activity of the other kinases, or alternatively another factor could upregulate both ERK kinase persistence and the activity of the other kinases. We next stimulated NIH/3T3 cells with forskolin. Forskolin preferentially induced PKA activity, inducing the other three kinases to a lesser degree (Figures S5C–S5E), consistent with previous results.[2,45,46] Thus, TMI allows for many kinases to be imaged at once, facilitating examination of their relationships to one another and enabling hypotheses to be generated about the nature of their interaction. Future studies systematically mapping out how kinases work together in networks could help with the investigation of mechanisms underpinning many healthy processes and disease states.

Monitoring a large number of dynamic signals with combined temporally and spectrally multiplexed imaging in individual cells

TMI enables sets of expressed genes (Figures 3G and 4A–4C) or dynamical signals (Figures 4D–4H) to be simultaneously measured using a single color channel, which in turns frees up spectrum for additional measurements. We combined our TMI version of FUCCI4 with multispectral reporters, again based on the KTR principle, of cyclin-dependant kinases 2 (CDK2, based on TagBFP2)[47] and 4/6 (CDK4/6, based on mCherry)[48] (Figure 5A, left). Cell-cycle progression is cooperatively regulated by multiple CDKs and thus knowing how CDK activities proceed throughout each cell-cycle phase is critical to understanding cell-cycle regulation. Past results indicated that both CDK2 and CDK4/6 enter the M phase with a high level of activity, which drops rapidly during mitosis until the cell reaches early G1 phase, followed by a slow buildup of activity throughout G1 phase (Figure 5A, right).[47–50] Although it was known that both CDK2 and CDK4/6 activities are higher at the end of G2 phase than at the beginning of S phase,[47,48] how CDK2 and CDK4/6 activities change throughout S and G2 were unknown. Here, enabled by TMI-based FUCCI4, we were able to observe how CDK2 and CDK4/6 activities change in all four cell-cycle phases in NIH/3T3 cells (Figure 5B; with additional examples in Figure S6A). We replicated prior observations that CDK2 and CDK4/6 activity went through an abrupt drop in M phase, reaching a maximum dip in early G1, and then started to build up throughout G1 (Figures 5C and 5D). In addition, we found that after entering S phase, CDK2 activity kept rising at a slow rate (Figure 5C; with additional analysis in Figure S5B); the rise continued during G2, until reaching the peak observed in early M phase (Figures 5C and 5E). However, CDK4/6 activity exhibited a different pattern. It plateaued throughout S phase, only beginning to increase when G2 began (Figures 5D and 5E). Thus, TMI may be useful for teasing apart the way multiple signals work together to govern cell-cycle regulation.

As another example of TMI being used in conjunction with multicolor imaging, we combined the four previously mentioned green FP-based KTRs with a near-infrared Ca^{2+} indicator (NIR-GECO2G),[51] a red fluorescent cyclic adenosine monophosphate (cAMP) indicator (Pink Flamindo),[52] and a blue fluorescent protein kinase C (PKC) indicator (BlueCKAR),[2] with the goal of simultaneously observing JNK, ERK, P38, PKA, Ca^{2+}, cAMP, and PKC (Figure 5F). NIH/3T3 cells expressing all seven reporters were imaged before and after the addition of 50 μM forskolin, followed by the addition of 100 ng/mL phorbol 12-myristate 13-acetate (PMA) (without removal of the forskolin). Forskolin is known to induce substantial cAMP, Ca^{2+}, and PKA responses; lesser ERK, P38, and JNK responses; and no PKC response.[1,2] TMI imaging of all seven signals at once under forskolin challenge was consistent with these prior findings when data were averaged across all cells (Figure 5G). PMA is a commonly used PKC activator, but studies have shown that it could also activate PKA, cAMP, JNK, and ERK.[53,54] We found that when PMA was added, PKC showed a rise and PKA, cAMP, JNK, and ERK showed boosted responses, whereas P38 and Ca^{2+} exhibited no change and possibly a decline, when data were averaged across all cells (Figure 5G). As above, we wondered if detailed examination of the relationship between specific signals, performed in individual cells, might reveal novel patterns and perhaps hypotheses of how these signals interact. We again note that these patterns are examples of the kind of observation TMI empowers and do not intend this as a full scientific study, which would require extensive experiments beyond the scope of this technology

(I–L) Comparisons of averaged ERK (I), JNK (J), P38 (K), and PKA (L) activity between type 1 and type 2 NIH/3T3 cells. The data are the same as in (H). For ERK, Wilcoxon rank-sum tests were run for the averaged amplitudes between type 1 and type 2 from t = 28 to t = 34 min (double arrows), and the averaged values from t = 18 to 24 min and t = 48 to t = 54 min for both type 1 (red line) and type 2 cells (blue line). For JNK, P38, and PKA, Wilcoxon rank-sum tests were run for the averaged amplitudes between type 1 and type 2 cells from t = 28 to t = 34 min (double arrows). Throughout the figure: *p < 0.05, **p < 0.01, ***p < 0.001, and ****p < 0.0001; n.s., no significance.
See also Figure S4 and S5.

Please cite this article in press as: Qian et al., Temporally multiplexed imaging of dynamic signaling networks in living cells, Cell (2023), https://doi.org/10.1016/j.cell.2023.11.010

CellPress
OPEN ACCESS

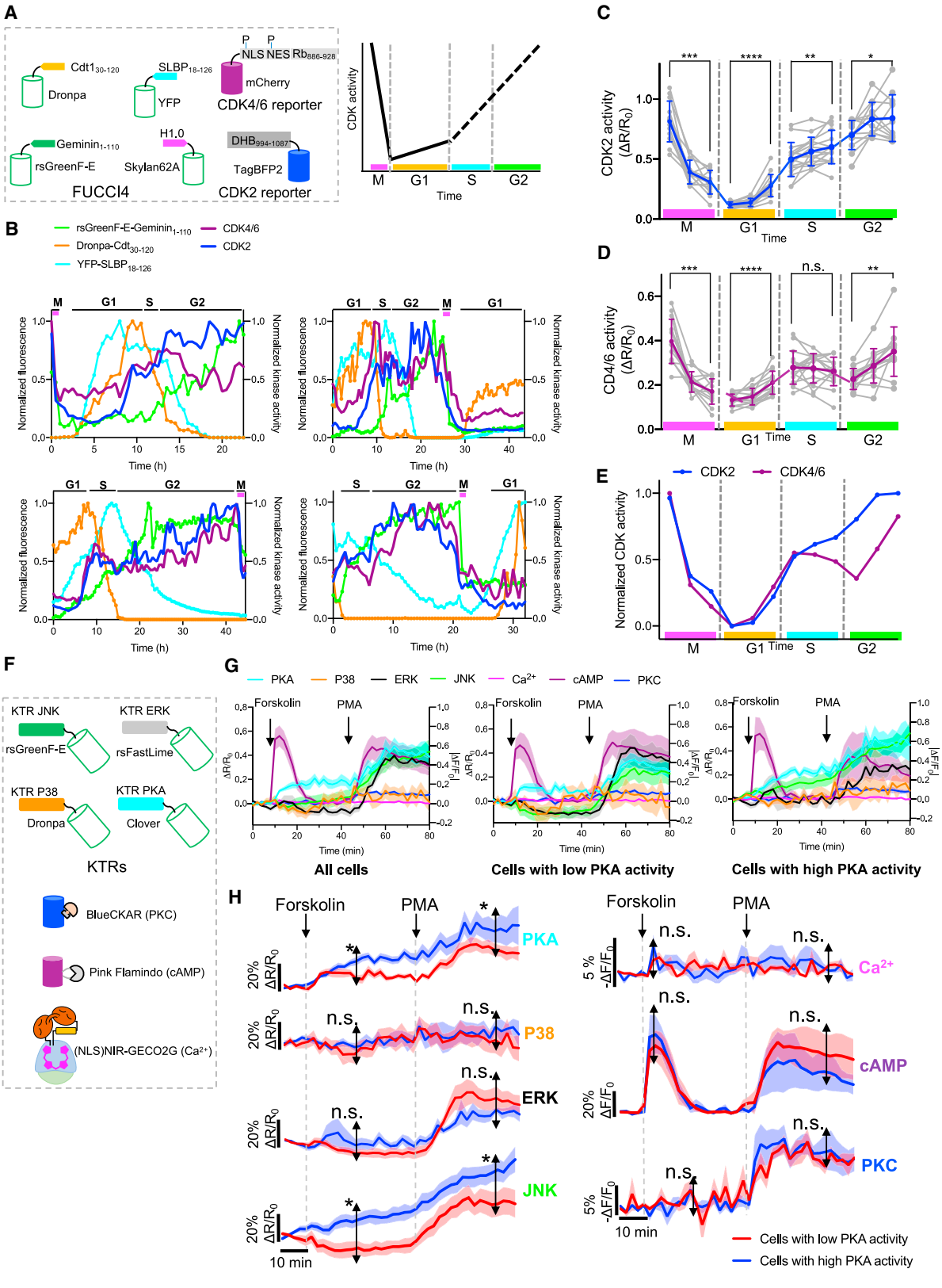

(legend on next page)

Please cite this article in press as: Qian et al., Temporally multiplexed imaging of dynamic signaling networks in living cells, Cell (2023), https://doi.org/10.1016/j.cell.2023.11.010

paper. With that in mind, we grouped the cells into two categories: cells with low PKA activity ($(\Delta R/R_0)$max under forskolin stimulation <0.2) and cells with high PKA activity ($(\Delta R/R_0)$max under forskolin stimulation $\geq$ 0.2) (Figures 5G and 5H; with raw traces in Figures S6C and S6D). Comparing the cells with high vs. low PKA activity, we found that JNK activity exhibited a correlation with PKA activity, whereas the other signals did not (Figures 5G, 5H, S6C, and S6D). This leads to a potential hypothesis where PKA reinforces JNK or the other way around—or, perhaps, a third factor upregulates both—at least in this cell type and pharmacological context. Such a hypothesis could be tested further via traditional biological methodologies, if so desired. Thus, by combining spectral and temporal multiplexing we were able to image seven different signals, in individual cells, revealing potential relationships between them—to our knowledge, more than previously possible with fully genetically encoded indicators being imaged in living cells on conventional fluorescent microscopes.

Practical considerations of TMI

As when any technology enters a laboratory, it is useful to think about how end users can use TMI in the most practical way. First, TMI relies on repeatable photoswitching of rsFPs (we note that protein fusion of an rsFP to a target protein, formaldehyde fixation of an rsFP, or expression of an rsFP in a different cell line did not change the photoswitching rates of the rsFP; Figures S7A and S7B), and thus even illumination of specimens is helpful for accurate signal unmixing (the illumination patterns used in this study were even, and thus we only measured one reference trace for each fluorophore, across the entire image). If uneven illumination cannot be avoided, in principle one could measure the reference trace on a pixel-by-pixel basis on control samples. Second, since the processing of brief movies is done pixel by pixel, movement of imaging samples during photoswitching should be avoided; if movement occurs, image registration might be needed. Third, the imaging time for each brief movie, in the current study, ranged from 3 to 15 s in most cases, depending on illumination intensity and fluorophore choice; in principle, stronger excitation could be used if a shorter time duration for the brief movie was preferred. To determine how short TMI movies could be, we did TMI simulations after measuring the off-switching traces of each of six green FPs obtained under 488 nm illumination at 55 mW/mm^2 (the highest power intensity on our spinning disk confocal microscope; Figure 6A). We found that when 3 FPs were used, only 20 frames (0.5 s) were required to have <4% crosstalk; with 4 FPs, 40 frames (1 s) were required; with 5 or 6 FPs, 60 frames (1.5 s) were required (Figure 6B). These results set the practically achievable temporal precision of TMI (e.g., TMI would not be currently useful for voltage imaging, which requires millisecond precision). We also measured the practical minimum duration of the inter-movie interval and found that on our hardware, TMI movies could easily be acquired with a 5-s interval (Figures 6C–6E show an example where subcellular organelles bear three FPs, and 0.5-s brief movies yield expected organelle shapes). Fourth, a brief movie must contain sufficient data for an accurate linear unmixing to be performed, comprising a certain minimum number of frames and sufficient fluorescence decrease over those frames. As noted above and in Figures 6A and 6B, using more intense illumination will enable faster fluorescence decline, and the number of frames over which the decline occurs will occur in a shorter amount of time, perhaps at the expense of greater photodamage. To balance these competing criteria, we recommend starting the design of an experiment with a 20- to 30-frame movie for TMI of 3 FPs, with an illumination intensity of 3.2 mW/mm^2 for green FPs (under such illumination conditions, the fluorescence intensity of Dronpa decreased by $\geq$30% at the end of the brief movie) and an illumination intensity of 9.4 mW/mm^2 for red FPs (under such illumination conditions, the fluorescence intensity of rScarlet decreased by $\geq$20% at the end of the brief movie). For TMI of 4 FPs, a 40- to 60-frame movie is recommended (at 3.2 for green and 9.4 mW/mm^2 for red, the fluorescence intensity of Dronpa decreased by $\geq$50% at the end of the brief movie utilized for green FPs, and the fluorescence intensity of rScarlet decreased by $\geq$30% at the end of the brief movie utilized for red FPs). For TMI of 5 or 6 FPs, a 60- to 80-frame movie is recommended to be acquired (at 3.2 mW/mm^2 for green, the fluorescence intensity of Dronpa decreased by $\geq$60% at the end of the brief movie; multiplexing of 5 or more red FPs is not currently possible because of the limited number of red rsFPs available). These recommended frame numbers and light powers are just starting points for experimental design, of course; if the signal is too dim or faster time resolution is desired, illumination intensity could be

Figure 5. Combined TMI and spectral multiplexing for imaging of many signals within living cells

(A–D) Simultaneous observation of cell-cycle phase changes and kinase activity. (A) Left, diagram of combined use of TMI-based FUCCI4 with CDK2 and CDK4/6 reporters (three plasmids were used: CMV::rsGreenFast-Geminin$_{1-110}$-P2A-Dronpa-Cdt$_{30-120}$-IRES-H1-Skylan62A-P2A-YFP-SLBP$_{18-126}$, EF1α::mCherry-CDK4KTR, and EF1α::DHB-TagBFP2). Right, schematic of CDK activity in different cell-cycle phases. (B) Representative traces of TMI-based FUCCI4 and CDK signaling, over the cell cycle. Traces of four dividing NIH/3T3 cells are shown. More raw traces, Figure S6A. (C and D) Plots of CDK2 (C) and CDK4/6 (D) activity as a function of each cell-cycle phase, without normalization. Mean ± SD, individual values plotted as dots (gray; dots from the same cell are connected); n = 25 cells from 5 culture batches (not all cells exhibited all complete phases). Wilcoxon signed-rank test with Holm-Bonferroni correction, ****p < 0.0001, ***p < 0.001, **p < 0.01, and *p < 0.05; n.s., no significance.

(E) Superimposed plots of CDK2 and CDK4/6 activity (from C and D, and normalized to 0–1).

(F–H) Simultaneous imaging of seven signals within single NIH/3T3 cells. (F) Reporters used (four plasmids were used: GAG::JNKKTR-rsGreenF-E-P2A-ERKKTR-rsFastLime-IRES-PKAKTR-Clover-P2A-P38KTR-Dropna, CMV::BlueCKAR, CMV::Pink Flamindo, and CAG::NLS-NIR-GECO2G). (G) Averaged signals of PKA (cyan), P38 (orange), ERK (black), JNK (green), Ca^{2+} (magenta), cAMP (purple), and PKC (blue) from all NIH/3T3 cells (left); cells with low PKA activity (middle; as defined in the text) and cells with high PKA activity (right) under stimulation with 50 μM forskolin followed by 100 ng/mL PMA; n = 9 cells (5 cells with low PKA activity and 4 cells with high PKA activity) from 2 culture batches. Mean ± SEM. (H) Comparisons of PKA, P38, ERK, JNK, Ca^{2+}, cAMP, and PKC between cells with low PKA activity and cells with high PKA activity (data from G). Wilcoxon rank-sum tests, *p < 0.05; n.s., significance.

See also Figure S6.

Please cite this article in press as: Qian et al., Temporally multiplexed imaging of dynamic signaling networks in living cells, Cell (2023), https://doi.org/10.1016/j.cell.2023.11.010

CellPress
OPEN ACCESS

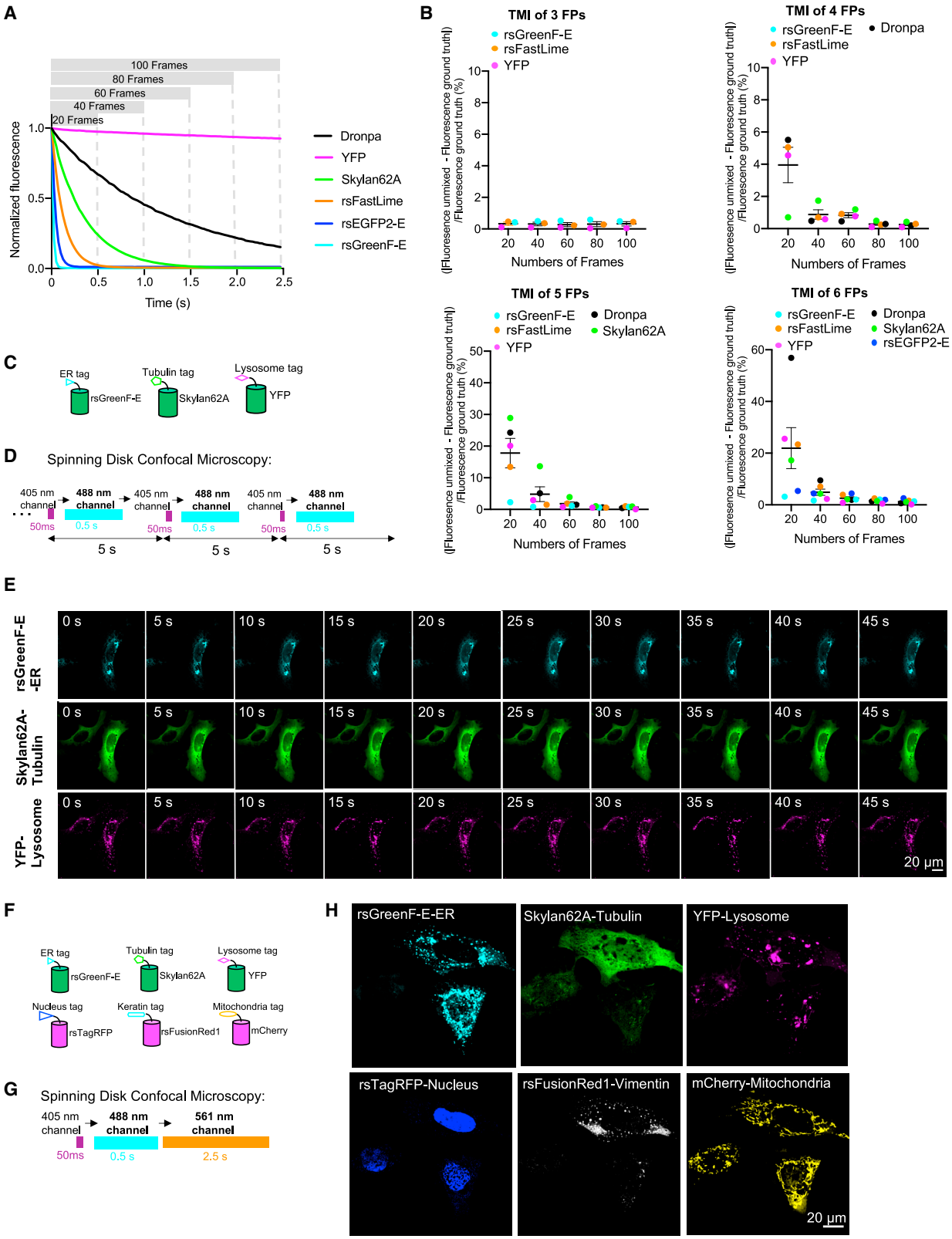

(legend on next page)

Please cite this article in press as: Qian et al., Temporally multiplexed imaging of dynamic signaling networks in living cells, Cell (2023), https://doi.org/10.1016/j.cell.2023.11.010

increased, perhaps iteratively optimizing light power and time resolution when a signal is being explored for the first time (see Table 1 for characteristics of the FPs used in this study and Table S1 for guidelines regarding time resolution of TMI vs. illumination intensity, for experiment planning). Fifth, even though rsFPs can resume brightly fluorescing, with minimal loss, after each round of off-switching,[20–22,26,27,55] photobleaching of most FPs in TMI was somewhat larger than seen in conventional imaging (Figures S7C and S7E), owing to the prolonged illumination needed to take enough brief movies to extract a time series dataset from living cells. Importantly, photobleaching does not substantially change the off-switching behaviors of rsFPs in our experiments (Figures S7D and S7F), key for TMI signal unmixing, and TMI signals appeared high quality even after normal amounts of photobleaching accumulated. Sixth, TMI is orthogonal to conventional spectrally multiplexed imaging. We did not observe bleed-through from red FPs to the green channel or from green FPs to the red channel on our microscopes; thus, multicolor TMI is possible; see Figures 6F–6H for an example of TMI with three red rsFPs and three green rsFPs, fused to different organelle- or cytoskeleton-targeting structures. In such cases, we recommend imaging green FPs right before red FPs, so that the excitation of green FPs works as an on-switch for red rsFPs. TMI reporters can also be combined with conventional fluorescent reporters, of course; acquiring images starting with the shortest-wavelength channel and ending with the longest-wavelength channel will enable excitation of shorter-wavelength fluorophores to turn on subsequently imaged rsFPs (see flowcharts in Figures S7G–S7J). Seventh, TMI could in principle be applied to 3D/volumetric imaging, although we performed 2D imaging here. We would recommend an initial experimental design of recording brief movies for each imaging plane one at a time, moving to new Z planes after applying a fresh on-switch light pulse each time to maximize signal. Eighth, off-switching kinetics of rsFPs are consistent when imaged on the same microscope, using the same acquisition parameters, over long periods of time (Figure S7K); thus, one calibration may be sufficient for experiments on a given microscope as long as the optical conditions remains constant. We recommend calibrating the kinetics of rsFPs again when performing experiments on new microscopes, especially for those with distinct illumination systems (e.g., light-emitting diode [LED] lights have broader spectral width than laser sources and thus will yield different results). If wavelengths and power intensities of illumination are close enough, then rsFPs will exhibit similar switching kinetics even on different microscopes (Figure S7L). In practice, it may be easier simply to obtain a new calibration curve than to count on illumination hardware and settings matching precisely; in the early days of a given lab using TMI, one may want to perform calibration often as a positive control to make sure everything is working properly. Finally, off-switching of rsFPs is well-fit by a one-component exponential decay. To be able to unmix rsFPs accurately in TMI, their time constants of off-switching have to be far enough apart to be easily distinguished. We found (Figures S1L and S3I) that rsFPs with ln(K) differences (K, time constant; ln, natural logarithm) larger than 1 (calibration conditions: illumination of 488 nm at 40 mW/mm^2 for green rsFPs and 561 nm at 50 mW/mm^2 for red rsFPs) offered acceptable separations, as used throughout this study.

DISCUSSION

TMI is an easy-to-use, powerful, versatile, and inexpensive strategy for imaging potentially arbitrary numbers of signals in living cells by taking advantage of the clocklike temporal properties of certain FPs. TMI enables both functional and structural imaging of live specimens on either standard epifluorescence microscopes or confocal microscopes, commonly available in biology labs. TMI only uses fully genetically encoded tools and thus fits into existing molecular and transgenic workflows without requiring chemical supplements for use. We identified potential relationships between the activities of different kinases in a cell line, showing how TMI can be used to generate hypotheses about the interaction of signaling molecules within cells. We were able to observe many signals at once in individual cells, even using a single color channel, thus freeing up spectrum for imaging other signals. This ability enabled us to discover potential relationships between CDK2 and CDK4/6 at specific phases in the cell cycle.

Compared with FLIM, spectral deconvolution, and Raman spectroscopy, TMI requires no hardware beyond those found on standard fluorescence microscopes, while achieving similar accuracy to FLIM and spectral deconvolution (e.g., crosstalk of TMI, FLIM, and spectral deconvolution are all in the few percent range).[3,8,57] Moreover, TMI uses fully genetically encoded FPs and can be combined with existing genetically encoded fluorescent reporters (e.g., using one optical channel for TMI of several signals and the others for imaging of Ca^{2+} or other activities using classical fluorescent reporters). The lack of requirement for chemical supplementation makes it easy for users to implement TMI with existing genetic and live-cell imaging workflows common in biology. Compared with SMI, using for example our signaling reporter island (SiRI) strategy,[1] TMI enables imaging of freely moving proteins rather than protein clusters fixed in

Figure 6. TMI supports faster imaging and simultaneous use of green and red rsFPs

(A) Reference traces of FPs under strong illumination (488-nm laser, 55 mW/mm^2), with different numbers of frames indicated by the gray dashed lines, for scale.

(B) Crosstalk of unmixed FP signals when 3–6 FPs were multiplexed, and acquired with varying frame numbers, when simulated using the references traces of (A), as in Figure 2F, etc.

(C–E) Fast TMI imaging, showing accurate reconstruction of three subcellular structures in living U2OS cells. (C) FPs used to visualize different cellular structures. (D) Imaging acquisition flowchart. (E) Representative images (out of three fields-of-view from one cell culture) of U2OS cells co-expressing constructs of (C), imaged as in (D).

(F–H) TMI imaging of subcellular structures of live U2OS cells using both green and red rsFPs. (F) FPs used to visualize different cellular structures. (G) Imaging acquisition flowchart. (H) Representative images (out of three fields-of-view from one cell culture) of U2OS cells co-expressing constructs of (F).

See also Figure S7.

Please cite this article in press as: Qian et al., Temporally multiplexed imaging of dynamic signaling networks in living cells, Cell (2023), https://doi.org/10.1016/j.cell.2023.11.010

CellPress
OPEN ACCESS

Table 1. Spectroscopic characteristics of FPs used for TMI in this work

FP	Excitation peak (nm)	Emission peak (nm)	Extinction coefficient ($\times 10^3$ M^{-1} cm^{-1})	Quantum yield	Brightness	Switch-off half time (s)[j]
rsGreenF-E[a]	485	511	66	0.39	25.74	0.02273
rsEGFP2-E[b]	493	510	47	0.36	16.92	0.05233
rsFastLime[c]	496	518	39	0.77	30.03	0.1961
Skylan62A	502	514	84	0.61	51.53	0.4189
Dronpa[d]	503	518	95	0.85	80.75	1.546
YFP[e]	513	527	67	0.67	44.89	N/A
Clover[f]	505	515	111	0.67	84.36	N/A
rsTagRFP[g]	567	585	37	0.11	4.05	0.3928
rsFusionRed1[h]	577	605	82	0.1	8.24	0.9587
rScarlet	570	592	61	0.44	26.97	3.035
mCherry[i]	587	610	72	0.22	15.84	N/A

Brightness is defined as the product of extinction coefficient and quantum yield.
N/A, not applicable.
[a]Data from Roebroek et al.[22]
[b]Data from Grotjohann et al.[24]
[c]Data from Stiel et al.[21]
[d]Data from Ando et al.[20]
[e]Data from Ormö et al.[25]
[f]Data from Lam et al.[56]
[g]Data from Pletnev et al.[26]
[h]Data from Pennacchietti et al.[27]
[i]Data from Shaner et al.[31]
[j]Measured in NIH/3T3 cells under continuous illumination (green rsFPs: 488 nm at 40 mW/mm^2; red rsFPs: 561 nm at 50 mW/mm^2).

space, and it thus enables imaging of cell structures, changes in protein concentration, and protein translocation. One previous study utilized different photobleaching rates of spectrally similar fluorescent dyes to facilitate signal unmixing and successfully reconstructed snapshot images of three organelles in fixed cells.[19] However, photobleaching is an irreversible process, precluding imaging of signaling dynamics in living cells; furthermore, it requires strong illumination and results in photodamage, which makes it undesirable for live imaging. Some recent studies classified bacteria expressing distinct rsFPs by delivering excitation pulse sequences varying in number and/or light intensity.[58,59] Those methods were shown to discriminate entire bacteria as discrete entities but were not used to yield images of individual cells expressing multiple rsFPs, which would be required, with low crosstalk, to perform multiplexed imaging of a living cell's signals.

Any new technology should raise questions about its safety and performance. We found that cells expressing multiple TMI constructs had similar exogenous protein expression levels to those expressing only one construct. In this study, we found no detectable phototoxicity or photo-induced signaling artifacts, pointing toward TMI being a safe and reliable method for measuring many cellular signals at once. Future endeavors could computationally optimize the signal unmixing algorithm for higher accuracy and/or faster computing, improve the photostability (including fluorescence stability and consistency of photoswitching behaviors of rsFPs after hundreds or thousands of switching cycles) and the brightness of currently available rsFPs, and develop far-red or NIR rsFPs to minimize the use of purple/blue/cyan light. Functional indicators of calcium and other cellular messengers could be developed based on rsFPs in order to broaden the kind of signals measurable with TMI. If bright photoswitchable small molecule fluorescent dyes were adapted for TMI, TMI could serve roles in other technology areas, e.g., multiplexed immunofluorescence imaging (although, one may need to optimize the chemical environment for consistent photoswitching of some fluorescent dyes[60]). TMI in non-transparent tissues, such as mammalian brain, and *in vivo* may also be of use; reversible saturable optical fluorescence transitions (RESOLFT), a super-resolution technique based on rsFPs, has been successfully used in mouse brain slices.[61] In summary, TMI is not only an immediately practical technique for biological imaging, but it can be adapted by the community in many directions.

Limitations of the study

As discussed above, TMI is currently not favorable for detecting fast-changing dynamics happening in <0.5 s: TMI requires a 20- to 70-frame brief movie to be acquired to multiplex 3–6 FPs per color channel, which means that the temporal resolution of TMI ranges from 0.5 to 15 s, depending on excitation power intensity. Note that for fast TMI imaging, the intense illumination required should be carefully considered for any potential side effects—while such light powers are routinely used in fields like optogenetics[62] and voltage imaging,[63] careful controls should of course be done in any new experimental context to make sure that such illumination does not interfere with the biology under investigation. Although the time cost of TMI is comparable to that of

Please cite this article in press as: Qian et al., Temporally multiplexed imaging of dynamic signaling networks in living cells, Cell (2023), https://doi.org/10.1016/j.cell.2023.11.010

spectrally multiplexed imaging performed under standard microscopes equipped with one camera and light source (where multicolor images are taken sequentially; Table S2), theoretically, if multiple cameras are used and proper accessory optics chosen, then spectrally multiplexed imaging can acquire multicolor images simultaneously rather than sequentially, and then it would be 20–70 times faster than TMI. TMI is also slower than recently described versions of FLIM and spectral deconvolution, whose time resolution ranges from dozens of milliseconds to hundreds of milliseconds.[3,64] In principle, TMI of three FPs with a brief movie duration, and thus time resolution of ~0.5 s, is able to detect signals changing over a few seconds. But, importantly, during the 0.5 s of acquisition time for the brief movie, the biological signal should be stable for standard linear unmixing to work. That means signals should be bandlimited, i.e., not changing faster than the time over which a brief movie is acquired. This bandlimiting could be biological, e.g., the biological system itself does not change quickly, or it could be sensor dependent, e.g., the sensor might not be able to change faster than a certain rate. For some signals, the development of new types of sensors for TMI may be needed. For example, one could not use an existing fluorescent voltage indicator for TMI imaging, both because the fluorophores utilized in such indicators are not photoswitchable and because existing sensor designs are not appropriately bandlimited. We cannot rule out that new signal processing and/or machine learning strategies could overcome this limitation. Nevertheless, the kinds of applications we show for TMI in the existing paper, which rely on slower biological changes—monitoring subcellular structure and organelle shape, gene expression, protein translation, protein amount, protein location, and so forth—are immediately useful, even as future development of TMI tools has much room for growth. TMI also faces more photobleaching compared with conventional spectrally multiplexed imaging (although, thankfully, photobleaching does not substantially change the photoswitching behaviors of rsFPs, key for accurate TMI signal unmixing). Thus, choosing photostable FPs for TMI, and being aware of the photobleaching rates of the FPs used, would be helpful for experiments aiming for quantitative analysis.

STAR★METHODS

Detailed methods are provided in the online version of this paper and include the following:

SUPPLEMENTAL INFORMATION

Supplemental information can be found online at https://doi.org/10.1016/j.cell.2023.11.010.

ACKNOWLEDGMENTS

We thank Panagiotis Symvoulidis for help with imaging setup and Jordan Harrod, Yangning Lu, and Bobae An for initial concept testing and useful discussions. We also thank Chi Zhang for cell culture preparation. Z.W. acknowledges Alana Fellowship. E.S.B. was supported by Lisa Yang, Ashar Aziz, K. Lisa Yang and Hock E. Tan Center for Molecular Therapeutics at MIT, John Doerr, Jed McCaleb, James Fickel, HHMI, NIH 1R01MH123977, NIH 1R01AG070831, NIH RF1NS113287, NIH R01MH122971, NIH R01DA029639, NIH UF1NS107697, and NIH 1R01MH114031.

AUTHOR CONTRIBUTIONS

Y.Q. and E.S.B. conceived the project, designed the experiments, interpreted the data, and wrote the paper. Y.Q. developed Skylan62A and rScarlet. O.T.C. and Z.W. wrote the code for TMI signal unmixing and TMI simulations. Y.Q. performed experiments in cultured cells. Y.Q., Z.W., and B.G.-A. performed experiments in zebrafish. Y.Q. performed data analysis. E.S.B. supervised the project.

DECLARATION OF INTERESTS

E.S.B. and Y.Q. have applied for a patent on the technology, assigned to MIT.

Received: March 6, 2023
Revised: July 30, 2023
Accepted: November 5, 2023
Published: November 28, 2023

REFERENCES

1. Linghu, C., Johnson, S.L., Valdes, P.A., Shemesh, O.A., Park, W.M., Park, D., Piatkevich, K.D., Wassie, A.T., Liu, Y., An, B., et al. (2020). Spatial multiplexing of fluorescent reporters for imaging signaling network dynamics. Cell *183*, 1682–1698.e24. https://doi.org/10.1016/j.cell.2020.10.035.
2. Mehta, S., Zhang, Y., Roth, R.H., Zhang, J.F., Mo, A., Tenner, B., Huganir, R.L., and Zhang, J. (2018). Single-fluorophore biosensors for sensitive and multiplexed detection of signalling activities. Nat. Cell Biol. *20*, 1215–1225. https://doi.org/10.1038/s41556-018-0200-6.
3. Chen, K., Yan, R., Xiang, L., and Xu, K. (2021). Excitation spectral microscopy for highly multiplexed fluorescence imaging and quantitative biosensing. Light Sci. Appl. *10*, 97. https://doi.org/10.1038/s41377-021-00536-3.
4. Shcherbakova, D.M., Stepanenko, O.V., Turoverov, K.K., and Verkhusha, V.V. (2018). Near-infrared fluorescent proteins: multiplexing and

Please cite this article in press as: Qian et al., Temporally multiplexed imaging of dynamic signaling networks in living cells, Cell (2023), https://doi.org/10.1016/j.cell.2023.11.010

optogenetics across scales. Trends Biotechnol. *36*, 1230–1243. https://doi.org/10.1016/j.tibtech.2018.06.011.

5. Liu, A.M.F., Lo, R.K.H., Wong, C.S.S., Morris, C., Wise, H., and Wong, Y.H. (2006). Activation of STAT3 by Gαs distinctively requires protein kinase A, JNK, and phosphatidylinositol 3-kinase. J. Biol. Chem. *281*, 35812–35825. https://doi.org/10.1074/jbc.M605288200.
6. Melling, C.W.J., Krause, M.P., and Noble, E.G. (2006). PKA-mediated ERK1/2 inactivation and hsp70 gene expression following exercise. J. Mol. Cell. Cardiol. *41*, 816–822. https://doi.org/10.1016/j.yjmcc.2006.05.010.
7. Wang, J.Q., Fibuch, E.E., and Mao, L. (2007). Regulation of mitogen-activated protein kinases by glutamate receptors. J. Neurochem. *100*, 1–11. https://doi.org/10.1111/j.1471-4159.2006.04208.x.
8. Merchant, F.A., and Castleman, K.R. (2009). Chapter 27. Computer-assisted microscopy. In The Essential Guide to Image Processing, A. Bovik, ed. (Academic Press), pp. 777–831. https://doi.org/10.1016/B978-0-12-374457-9.00027-5.
9. Higuchi-Sanabria, R., Garcia, E.J., Tomoiaga, D., Munteanu, E.L., Feinstein, P., and Pon, L.A. (2016). Characterization of fluorescent proteins for three- and four-color live-cell imaging in S. cerevisiae. PLoS One *11*, e0146120. https://doi.org/10.1371/journal.pone.0146120.
10. Gregor, I., and Patting, M. (2015). Pattern-based linear unmixing for efficient and reliable analysis of multicomponent TCSPC data. In Advanced Photon Counting: Applications, Methods, Instrumentation, P. Kapusta, M. Wahl, and R. Erdmann, eds. (Springer International Publishing), pp. 241–263. https://doi.org/10.1007/4243_2014_70.
11. Niehörster, T., Löschberger, A., Gregor, I., Krämer, B., Rahn, H.-J., Patting, M., Koberling, F., Enderlein, J., and Sauer, M. (2016). Multi-target spectrally resolved fluorescence lifetime imaging microscopy. Nat. Methods *13*, 257–262. https://doi.org/10.1038/nmeth.3740.
12. Frei, M.S., Tarnawski, M., Roberti, M.J., Koch, B., Hiblot, J., and Johnsson, K. (2022). Engineered HaloTag variants for fluorescence lifetime multiplexing. Nat. Methods *19*, 65–70. https://doi.org/10.1038/s41592-021-01341-x.
13. Tsurui, H., Nishimura, H., Hattori, S., Hirose, S., Okumura, K., and Shirai, T. (2000). Seven-color fluorescence imaging of tissue samples based on Fourier spectroscopy and singular value decomposition. J. Histochem. Cytochem. *48*, 653–662. https://doi.org/10.1177/002215540004800509.
14. Dorozynska, K., Ek, S., Kornienko, V., Andersson, D., Andersson, A., Ehn, A., and Kristensson, E. (2021). Snapshot multicolor fluorescence imaging using double multiplexing of excitation and emission on a single detector. Sci. Rep. *11*, 20454. https://doi.org/10.1038/s41598-021-99670-6.
15. Hu, F., Zeng, C., Long, R., Miao, Y., Wei, L., Xu, Q., and Min, W. (2018). Supermultiplexed optical imaging and barcoding with engineered polyynes. Nat. Methods *15*, 194–200. https://doi.org/10.1038/nmeth.4578.
16. Greenwald, E.C., Mehta, S., and Zhang, J. (2018). Genetically encoded fluorescent biosensors illuminate the spatiotemporal regulation of signaling networks. Chem. Rev. *118*, 11707–11794. https://doi.org/10.1021/acs.chemrev.8b00333.
17. Knöpfel, T., and Song, C. (2019). Optical voltage imaging in neurons: moving from technology development to practical tool. Nat. Rev. Neurosci. *20*, 719–727. https://doi.org/10.1038/s41583-019-0231-4.
18. Chen, F., Tillberg, P.W., and Boyden, E.S. (2015). Optical imaging. Expansion microscopy. Science *347*, 543–548. https://doi.org/10.1126/science.1260088.
19. Orth, A., Ghosh, R.N., Wilson, E.R., Doughney, T., Brown, H., Reineck, P., Thompson, J.G., and Gibson, B.C. (2018). Super-multiplexed fluorescence microscopy via photostability contrast. Biomed. Opt. Express *9*, 2943–2954. https://doi.org/10.1364/BOE.9.002943.
20. Ando, R., Mizuno, H., and Miyawaki, A. (2004). Regulated fast nucleocytoplasmic shuttling observed by reversible protein highlighting. Science *306*, 1370–1373. https://doi.org/10.1126/science.1102506.
21. Stiel, A.C., Trowitzsch, S., Weber, G., Andresen, M., Eggeling, C., Hell, S.W., Jakobs, S., and Wahl, M.C. (2007). 1.8 A bright-state structure of the reversibly switchable fluorescent protein Dronpa guides the generation of fast switching variants. Biochem. J. *402*, 35–42. https://doi.org/10.1042/BJ20061401.
22. Roebroek, T., Duwé, S., Vandenberg, W., and Dedecker, P. (2017). Reduced fluorescent protein switching fatigue by binding-induced emissive state stabilization. Int. J. Mol. Sci. *18*, 2015. https://doi.org/10.3390/ijms18092015.
23. Zhang, X., Zhang, M., Li, D., He, W., Peng, J., Betzig, E., and Xu, P. (2016). Highly photostable, reversibly photoswitchable fluorescent protein with high contrast ratio for live-cell superresolution microscopy. Proc. Natl. Acad. Sci. USA *113*, 10364–10369. https://doi.org/10.1073/pnas.1611038113.
24. Grotjohann, T., Testa, I., Reuss, M., Brakemann, T., Eggeling, C., Hell, S.W., and Jakobs, S. (2012). rsEGFP2 enables fast RESOLFT nanoscopy of living cells. Elife *1*, e00248. https://doi.org/10.7554/eLife.00248.
25. Ormö, M., Cubitt, A.B., Kallio, K., Gross, L.A., Tsien, R.Y., and Remington, S.J. (1996). Crystal structure of the Aequorea victoria green fluorescent protein. Science *273*, 1392–1395. https://doi.org/10.1126/science.273.5280.1392.
26. Pletnev, S., Subach, F.V., Dauter, Z., Wlodawer, A., and Verkhusha, V.V. (2012). A structural basis for reversible photoswitching of absorbance spectra in red fluorescent protein rsTagRFP. J. Mol. Biol. *417*, 144–151. https://doi.org/10.1016/j.jmb.2012.01.044.
27. Pennacchietti, F., Serebrovskaya, E.O., Faro, A.R., Shemyakina, I.I., Bozhanova, N.G., Kotlobay, A.A., Gurskaya, N.G., Bodén, A., Dreier, J., Chudakov, D.M., et al. (2018). Fast reversibly photoswitching red fluorescent proteins for live-cell RESOLFT nanoscopy. Nat. Methods *15*, 601–604. https://doi.org/10.1038/s41592-018-0052-9.
28. Bindels, D.S., Haarbosch, L., van Weeren, L., Postma, M., Wiese, K.E., Mastop, M., Aumonier, S., Gotthard, G., Royant, A., Hink, M.A., et al. (2017). mScarlet: a bright monomeric red fluorescent protein for cellular imaging. Nat. Methods *14*, 53–56. https://doi.org/10.1038/nmeth.4074.
29. Stiel, A.C., Andresen, M., Bock, H., Hilbert, M., Schilde, J., Schönle, A., Eggeling, C., Egner, A., Hell, S.W., and Jakobs, S. (2008). Generation of monomeric reversibly switchable red fluorescent proteins for far-field fluorescence nanoscopy. Biophys. J. *95*, 2989–2997. https://doi.org/10.1529/biophysj.108.130146.
30. Lavoie-Cardinal, F., Jensen, N.A., Westphal, V., Stiel, A.C., Chmyrov, A., Bierwagen, J., Testa, I., Jakobs, S., and Hell, S.W. (2014). Two-color RESOLFT nanoscopy with green and red fluorescent photochromic proteins. ChemPhysChem *15*, 655–663. https://doi.org/10.1002/cphc.201301016.
31. Shaner, N.C., Campbell, R.E., Steinbach, P.A., Giepmans, B.N.G., Palmer, A.E., and Tsien, R.Y. (2004). Improved monomeric red, orange and yellow fluorescent proteins derived from Discosoma sp. red fluorescent protein. Nat. Biotechnol. *22*, 1567–1572. https://doi.org/10.1038/nbt1037.
32. Livet, J., Weissman, T.A., Kang, H., Draft, R.W., Lu, J., Bennis, R.A., Sanes, J.R., and Lichtman, J.W. (2007). Transgenic strategies for combinatorial expression of fluorescent proteins in the nervous system. Nature *450*, 56–62. https://doi.org/10.1038/nature06293.
33. Köster, R.W., and Fraser, S.E. (2001). Tracing transgene expression in living zebrafish embryos. Dev. Biol. *233*, 329–346. https://doi.org/10.1006/dbio.2001.0242.
34. Formella, I., Svahn, A.J., Radford, R.A.W., Don, E.K., Cole, N.J., Hogan, A., Lee, A., Chung, R.S., and Morsch, M. (2018). Real-time visualization of oxidative stress-mediated neurodegeneration of individual spinal motor neurons in vivo. Redox Biol. *19*, 226–234. https://doi.org/10.1016/j.redox.2018.08.011.
35. Bajar, B.T., Lam, A.J., Badiee, R.K., Oh, Y.-H., Chu, J., Zhou, X.X., Kim, N., Kim, B.B., Chung, M., Yablonovitch, A.L., et al. (2016). Fluorescent indicators for simultaneous reporting of all four cell cycle phases. Nat. Methods *13*, 993–996. https://doi.org/10.1038/nmeth.4045.

Please cite this article in press as: Qian et al., Temporally multiplexed imaging of dynamic signaling networks in living cells, Cell (2023), https://doi.org/10.1016/j.cell.2023.11.010

36. Sakaue-Sawano, A., Yo, M., Komatsu, N., Hiratsuka, T., Kogure, T., Hoshida, T., Goshima, N., Matsuda, M., Miyoshi, H., and Miyawaki, A. (2017). Genetically encoded tools for optical dissection of the mammalian cell cycle. Mol. Cell *68*, 626–640.e5. https://doi.org/10.1016/j.molcel.2017.10.001.

37. Regot, S., Hughey, J.J., Bajar, B.T., Carrasco, S., and Covert, M.W. (2014). High-sensitivity measurements of multiple kinase activities in live single cells. Cell *157*, 1724–1734. https://doi.org/10.1016/j.cell.2014.04.039.

38. Jia, B.Z., Qi, Y., David Wong-Campos, J., Megason, S.G., and Cohen, A.E. (2022). A bioelectrical phase transition patterns the first beats of a vertebrate heart. Preprint at bioRxiv. https://doi.org/10.1101/2022.12.06.519309.

39. Shemesh, O.A., Linghu, C., Piatkevich, K.D., Goodwin, D., Celiker, O.T., Gritton, H.J., Romano, M.F., Gao, R., Yu, C.-C.J., Tseng, H.-A., et al. (2020). Precision calcium imaging of dense neural populations via a cell-body-targeted calcium indicator. Neuron *107*, 470–486.e11. https://doi.org/10.1016/j.neuron.2020.05.029.

40. Dana, H., Sun, Y., Mohar, B., Hulse, B.K., Kerlin, A.M., Hasseman, J.P., Tsegaye, G., Tsang, A., Wong, A., Patel, R., et al. (2019). High-performance calcium sensors for imaging activity in neuronal populations and microcompartments. Nat. Methods *16*, 649–657. https://doi.org/10.1038/s41592-019-0435-6.

41. Pursiheimo, J.P., Jalkanen, M., Taskén, K., and Jaakkola, P. (2000). Involvement of protein kinase A in fibroblast growth factor-2-activated transcription. Proc. Natl. Acad. Sci. USA *97*, 168–173. https://doi.org/10.1073/pnas.97.1.168.

42. Lichtenstein, M.P., Madrigal, J.L.M., Pujol, A., and Galea, E. (2012). JNK/ERK/FAK mediate promigratory actions of basic fibroblast growth factor in astrocytes via CCL2 and COX2. Neurosignals. *20*, 86–102. https://doi.org/10.1159/000330805.

43. Kim, B.S., Park, J.-Y., Kang, H.-J., Kim, H.-J., and Lee, J. (2014). Fucoidan/FGF-2 induces angiogenesis through JNK- and p38-mediated activation of AKT/MMP-2 signalling. Biochem. Biophys. Res. Commun. *450*, 1333–1338. https://doi.org/10.1016/j.bbrc.2014.06.137.

44. Kanazawa, S., Fujiwara, T., Matsuzaki, S., Shingaki, K., Taniguchi, M., Miyata, S., Tohyama, M., Sakai, Y., Yano, K., Hosokawa, K., et al. (2010). bFGF regulates PI3-kinase-Rac1-JNK pathway and promotes fibroblast migration in wound healing. PLoS One *5*, e12228. https://doi.org/10.1371/journal.pone.0012228.

45. Park, K.H., Park, H.J., Shin, K.S., Choi, H.S., Kai, M., and Lee, M.K. (2012). Modulation of PC12 cell viability by forskolin-induced cyclic AMP levels through ERK and JNK pathways: an implication for L-dopa-induced cytotoxicity in nigrostriatal dopamine neurons. Toxicol. Sci. *128*, 247–257. https://doi.org/10.1093/toxsci/kfs139.

46. Delghandi, M.P., Johannessen, M., and Moens, U. (2005). The cAMP signalling pathway activates CREB through PKA, p38 and MSK1 in NIH 3T3 cells. Cell. Signal. *17*, 1343–1351. https://doi.org/10.1016/j.cellsig.2005.02.003.

47. Spencer, S.L., Cappell, S.D., Tsai, F.-C., Overton, K.W., Wang, C.L., and Meyer, T. (2013). The proliferation-quiescence decision is controlled by a bifurcation in CDK2 activity at mitotic exit. Cell *155*, 369–383. https://doi.org/10.1016/j.cell.2013.08.062.

48. Yang, H.W., Cappell, S.D., Jaimovich, A., Liu, C., Chung, M., Daigh, L.H., Pack, L.R., Fan, Y., Regot, S., Covert, M., et al. (2020). Stress-mediated exit to quiescence restricted by increasing persistence in CDK4/6 activation. eLife *9*, e44571. https://doi.org/10.7554/eLife.44571.

49. Stern, B., and Nurse, P. (1996). A quantitative model for the cdc2 control of S phase and mitosis in fission yeast. Trends Genet. *12*, 345–350. https://doi.org/10.1016/S0168-9525(96)80016-3.

50. Coudreuse, D., and Nurse, P. (2010). Driving the cell cycle with a minimal CDK control network. Nature *468*, 1074–1079. https://doi.org/10.1038/nature09543.

51. Qian, Y., Cosio, D.M.O., Piatkevich, K.D., Aufmkolk, S., Su, W.-C., Celiker, O.T., Schohl, A., Murdock, M.H., Aggarwal, A., Chang, Y.-F., et al. (2020). Improved genetically encoded near-infrared fluorescent calcium ion indicators for in vivo imaging. PLoS Biol. *18*, e3000965. https://doi.org/10.1371/journal.pbio.3000965.

52. Harada, K., Ito, M., Wang, X., Tanaka, M., Wongso, D., Konno, A., Hirai, H., Hirase, H., Tsuboi, T., and Kitaguchi, T. (2017). Red fluorescent protein-based cAMP indicator applicable to optogenetics and in vivo imaging. Sci. Rep. *7*, 7351. https://doi.org/10.1038/s41598-017-07820-6.

53. Baillie, G., MacKenzie, S.J., and Houslay, M.D. (2001). Phorbol 12-myristate 13-acetate triggers the protein kinase A-mediated phosphorylation and activation of the PDE4D5 cAMP phosphodiesterase in human aortic smooth muscle cells through a route involving extracellular signal regulated kinase (ERK). Mol. Pharmacol. *60*, 1100–1111. https://doi.org/10.1124/mol.60.5.1100.

54. Sriraman, V., Modi, S.R., Bodenburg, Y., Denner, L.A., and Urban, R.J. (2008). Identification of ERK and JNK as signaling mediators on protein kinase C activation in cultured granulosa cells. Mol. Cell. Endocrinol. *294*, 52–60. https://doi.org/10.1016/j.mce.2008.07.011.

55. Rosenbloom, A.B., Lee, S.H., To, M., Lee, A., Shin, J.Y., and Bustamante, C. (2014). Optimized two-color super resolution imaging of Drp1 during mitochondrial fission with a slow-switching Dronpa variant. Proc. Natl. Acad. Sci. USA *111*, 13093–13098. https://doi.org/10.1073/pnas.1320044111.

56. Lam, A.J., St-Pierre, F., Gong, Y., Marshall, J.D., Cranfill, P.J., Baird, M.A., McKeown, M.R., Wiedenmann, J., Davidson, M.W., Schnitzer, M.J., et al. (2012). Improving FRET dynamic range with bright green and red fluorescent proteins. Nat. Methods *9*, 1005–1012. https://doi.org/10.1038/nmeth.2171.

57. Vallmitjana, A., Dvornikov, A., Torrado, B., Jameson, D.M., Ranjit, S., and Gratton, E. (2020). Resolution of 4 components in the same pixel in FLIM images using the phasor approach. Methods Appl. Fluoresc. *8*, 035001. https://doi.org/10.1088/2050-6120/ab8570.

58. Valenta, H., Hugelier, S., Duwé, S., Lo Gerfo, G., Müller, M., Dedecker, P., and Vandenberg, W. (2021). Separation of spectrally overlapping fluorophores using intra-exposure excitation modulation. Biophys. Rep. (N Y) *1*, 100026. https://doi.org/10.1016/j.bpr.2021.100026.

59. Chouket, R., Pellissier-Tanon, A., Lahlou, A., Zhang, R., Kim, D., Plamont, M.-A., Zhang, M., Zhang, X., Xu, P., Desprat, N., et al. (2022). Extra kinetic dimensions for label discrimination. Nat. Commun. *13*, 1482. https://doi.org/10.1038/s41467-022-29172-0.

60. Chozinski, T.J., Gagnon, L.A., and Vaughan, J.C. (2014). Twinkle, twinkle little star: photoswitchable fluorophores for super-resolution imaging. FEBS Lett. *588*, 3603–3612. https://doi.org/10.1016/j.febslet.2014.06.043.

61. Testa, I., Urban, N.T., Jakobs, S., Eggeling, C., Willig, K.I., and Hell, S.W. (2012). Nanoscopy of living brain slices with low light levels. Neuron *75*, 992–1000. https://doi.org/10.1016/j.neuron.2012.07.028.

62. Stujenske, J.M., Spellman, T., and Gordon, J.A. (2015). Modeling the spatiotemporal dynamics of light and heat propagation for in vivo optogenetics. Cell Rep. *12*, 525–534. https://doi.org/10.1016/j.celrep.2015.06.036.

63. Villette, V., Chavarha, M., Dimov, I.K., Bradley, J., Pradhan, L., Mathieu, B., Evans, S.W., Chamberland, S., Shi, D., Yang, R., et al. (2019). Ultrafast two-photon imaging of a high-gain voltage indicator in awake behaving mice. Cell *179*, 1590–1608.e23. https://doi.org/10.1016/j.cell.2019.11.004.

64. Raspe, M., Kedziora, K.M., van den Broek, B., Zhao, Q., de Jong, S., Herz, J., Mastop, M., Goedhart, J., Gadella, T.W.J., Young, I.T., et al. (2016). siFLIM: single-image frequency-domain FLIM provides fast and photon-efficient lifetime data. Nat. Methods *13*, 501–504. https://doi.org/10.1038/nmeth.3836.

65. Sherer, N.M., Lehmann, M.J., Jimenez-Soto, L.F., Ingmundson, A., Horner, S.M., Cicchetti, G., Allen, P.G., Pypaert, M., Cunningham, J.M., and Mothes, W. (2003). Visualization of retroviral replication in living cells reveals budding into multivesicular bodies. Traffic *4*, 785–801. https://doi.org/10.1034/j.1600-0854.2003.00135.x.

Please cite this article in press as: Qian et al., Temporally multiplexed imaging of dynamic signaling networks in living cells, Cell (2023), https://doi.org/10.1016/j.cell.2023.11.010

66. Schmidt, U., Weigert, M., Broaddus, C., and Myers, G. (2018). Cell detection with star-convex polygons. In International Conference on Medical Image Computing and Computer-Assisted Intervention (Springer International Publishing), pp. 265–273. https://doi.org/10.1007/978-3-030-00934-2_30.

67. Gross, L.A., Baird, G.S., Hoffman, R.C., Baldridge, K.K., and Tsien, R.Y. (2000). The structure of the chromophore within DsRed, a red fluorescent protein from coral. Proc. Natl. Acad. Sci. USA *97*, 11990–11995. https://doi.org/10.1073/pnas.97.22.11990.

68. Kendall, J.M., Dormer, R.L., and Campbell, A.K. (1992). Targeting aequorin to the endoplasmic reticulum of living cells. Biochem. Biophys. Res. Commun. *189*, 1008–1016. https://doi.org/10.1016/0006-291x(92)92304-g.

69. Kimura, Y., Satou, C., and Higashijima, S.-I. (2008). V2a and V2b neurons are generated by the final divisions of pair-producing progenitors in the zebrafish spinal cord. Development *135*, 3001–3005. https://doi.org/10.1242/dev.024802.

70. Kwan, K.M., Fujimoto, E., Grabher, C., Mangum, B.D., Hardy, M.E., Campbell, D.S., Parant, J.M., Yost, H.J., Kanki, J.P., and Chien, C.-B. (2007). The Tol2kit: a multisite gateway-based construction kit for Tol2 transposon transgenesis constructs. Dev. Dyn. *236*, 3088–3099. https://doi.org/10.1002/dvdy.21343.

71. Fisher, S., Grice, E.A., Vinton, R.M., Bessling, S.L., Urasaki, A., Kawakami, K., and McCallion, A.S. (2006). Evaluating the biological relevance of putative enhancers using Tol2 transposon-mediated transgenesis in zebrafish. Nat. Protoc. *1*, 1297–1305. https://doi.org/10.1038/nprot.2006.230.

Please cite this article in press as: Qian et al., Temporally multiplexed imaging of dynamic signaling networks in living cells, Cell (2023), https://doi.org/10.1016/j.cell.2023.11.010

STAR★METHODS

KEY RESOURCES TABLE

REAGENT or RESOURCE	SOURCE	IDENTIFIER
Antibodies		
Anti-FLAG Antibody, Rabbit	Invitrogen, Thermo Fisher scientific	Cat# 740001; RRID: AB_2610628
Goat Anti-Rabbit IgG (H+L) Secondary Antibody, Alexa Fluor 647	Abcam	Cat# ab150079; RRID: AB_2722623
Chemicals, peptides, and recombinant proteins		
Forskolin	Thermo Fisher Scientific	Cat# J63292-MA
Mouse FGF basic Recombinant protein	R&D systems	Cat# 3139FB025
Phorbol 12-myristate 13-acetate (PMA)	Millipore Sigma	Cat# P8139
Dulbecco's Modified Eagle Media (DMEM)	GIBCO, Thermo Fisher Scientific	Cat# 11995040
Heat-inactivated fetal bovine serum	GIBCO, Thermo Fisher Scientific	Cat# A3840001
Penicillin/Streptomycin	GIBCO, Thermo Fisher Scientific	Cat# 15140-22
Opti-MEM	GIBCO, Thermo Fisher Scientific	Cat# 31-985-062
McCoy's 5A medium	GIBCO, Thermo Fisher Scientific	Cat# 16600082
10% bovine calf serum	Millipore Sigma	Cat# F4135
Pancuronium bromide	Millipore Sigma	Cat# P1918
MAXBlock Blocking medium	Active Motif	Cat# 15252
MAXStain Staining medium	Active Motif	Cat# 15253
MAXWash Washing medium	Active Motif	Cat# 15254
Critical Commencial Assays		
Lipofectamine 3000 transfection reagent	Invitrogen, Thermo Fisher Scientific	Cat# L3000008
TransIT-2020 Delivery system	Mirus Bio	Cat# MIR 5400
CellRox orange reagent	Thermo Fisher Scientific	Cat# 827C10443
NucleoSpin plasmid transfection-grade miniprep kit	Takara Bio	Cat# 740490
Deposited data		
Sequences of TMI-related DNA constructs	This paper	GenBank: OR636226, OR636227, OR652313, OR652314, OR652315, OR652316, OR652317, OR652318, OR652319
Code for TMI signal unmixing and TMI simulation	This paper	https://github.com/qiany09/Temporally-Multiplexed-Imaging
Experimental Models: Cell lines		
HEK293FT	Thermo Fiser Scientific	Cat# R70007
HeLa	ATCC	CCL-2
U2OS	ATCC	HTB-96
NIH/3T3	ATCC	CRL-1658
Recombinant DNA		
CMV::ER-rsGreenF-E-KDEL	This paper	N/A
CMV::H2B-rsEGFP2-E	This paper	N/A
CMV::mito-rsFastLime	This paper	N/A
CMV::Skylan62A-Tubulin	This paper	N/A
CMV::Dronpa-Alpha-Actin-19	Gift from Michael Davidson	Addgene plasmid# 57260
CMV::Lamp1-YFP	Sherer et al.[65]	Addgene plasmid# 1816
CMV::ER-rsGreenF-E-Flag-KDEL	This paper	N/A
CMV::H2B-rsEGFP2-E-Flag	This paper	N/A
CMV::mito-rsFastLime-Flag	This paper	N/A

(*Continued on next page*)

Please cite this article in press as: Qian et al., Temporally multiplexed imaging of dynamic signaling networks in living cells, Cell (2023), https://doi.org/10.1016/j.cell.2023.11.010

CellPress
OPEN ACCESS

Continued

REAGENT or RESOURCE	SOURCE	IDENTIFIER
CMV::Skylan62A-Flag-Tubulin	This paper	N/A
CMV::Dronpa-Flag-Alpha-Actin-19	This paper	N/A
CMV::Lamp1-YFP-Flag	This paper	N/A
CMV::H2B-rsTagRFP	This paper	N/A
CMV::rsFusionRed1-Vimentin	This paper	N/A
CMV::rScarlet-Alpha-Actin-19	This paper	N/A
CMV::Mito-mCherry	This paper	N/A
CMV::H2B-rsTagRFP-Flag	This paper	N/A
CMV::rsFusionRed1–Flag-Vimentin	This paper	N/A
CMV::rScarlet-Flg-Alpha-Actin-19	This paper	N/A
CMV::Mito-mCherry-Flag	This paper	N/A
CMV::rsGreenF-E	This paper	N/A
CMV::rsEGFP2-E	This paper	N/A
CMV::rsFastLime	This paper	N/A
CMV::Skylan62A	This paper	GenBank: OR636226
CMV::Dronpa	This paper	N/A
CMV::rsTagRFP	This paper	N/A
CMV::rsFusionRed1	This paper	N/A
CMV::rScarlet	This paper	GenBank: OR636227
10xUAS::rsTagRFP	This paper	N/A
10xUAS::rsFusionRed1	This paper	N/A
10xUAS::rScarlet	This paper	N/A
CMV::rsGreenF-E-Geminin$_{1-110}$ -IRES-Dronpa-Cdt$_{30-120}$	This paper	GenBank: OR652313, OR652314
CMV::YFP-SLBP$_{18-126}$-IRES-H1-Skylan62A	This paper	GenBank: OR652315, OR652316
CMV::P38KTR-Dronpa	This paper	GenBank: OR652317
PGK::JNKKTR-rsGreenF-E	This paper	GenBank: OR652318
CMV::ERKKTR-rsFastLime	This paper	GenBank: OR652319
PGK::PKAKTR-Clover	Regot et al.[37]	Addgene plasmid# 59153
GAG::JNKKTR-rsGreenF-E-P2A-ERKKTR-rsFastLime-IRES-PKAKTR-Clover-P2A-P38KTR-Dronpa	This paper	N/A
CMV::H2B-TagBFP2	This paper	N/A
CMV::rsGreenFast-Geminin$_{1-110}$-P2A-Dronpa-cdt$_{30-120}$-IRES-H1-Skylan62A-P2A-YFP-SLBP$_{18-126}$	This paper	N/A
EF1α::DHB-TagBFP2	This paper	N/A
EF1α::mCherry-CDK4KTR	Yang et al.[48]	Addgene plasmid# 126680
CMV::Pink Flamindo	Harada et al.[52]	Addgene plasmid# 102356
CAG::NLS-NIR-GECO2G	This paper	N/A
Software and Algorithms		
StarDist	Schmidt et al.[66]	https://imagej.net/plugins/stardist
ImageJ/Fiji	NIH/Fiji	https://fiji.sc
MATLAB	Mathworks	https://www.mathworks.com
Prism	Graphpad	https://www.graphpad.com/
Pymol	Schrödinger	https://pymol.org/
Origin 9.0	Origin Lab	https://www.originlab.com
NIS Element	Nikon	https://www.microscope.healthcare.nikon.com

(*Continued on next page*)

Please cite this article in press as: Qian et al., Temporally multiplexed imaging of dynamic signaling networks in living cells, Cell (2023), https://doi.org/10.1016/j.cell.2023.11.010

Continued

REAGENT or RESOURCE	SOURCE	IDENTIFIER
TMI signal unmixing	This paper	https://github.com/qiany09/Temporally-Multiplexed-Imaging
TMI simulation	This paper	https://github.com/qiany09/Temporally-Multiplexed-Imaging

RESOURCE AVAILABILITY

Lead contact

Further information and request for resources and reagent should be directed to and will be fulfilled by the lead contact, Edward S. Boyden (edboyden@mit.edu).

Materials availability

All relevant plasmids constructed in the work and their sequences are available from Addgene (Addgene plasmid # 205752 – 202766).

Data and code availability

- The accession numbers of TMI-related sequences generated in this paper are GenBank: OR636226, OR636227, OR652313, OR652314, OR652315, OR652316, OR652317, OR652318, OR652319.
- The code for TMI signal unmixing and TMI simulation is available at https://github.com/qiany09/Temporally-Multiplexed-Imaging.
- Any additional information required to reanalyze the data reported in this paper is available from the lead contact upon request.

EXPERIMENTAL MODEL AND STUDY PARTICIPANT DETAILS

Cell lines

HEK293FT cells (Thermo Fisher) and HeLa (ATCC) were grown and maintained in Dulbecco's modified Eagle's medium (DMEM) (Gibco) supplemented with 10% heat-inactivated fetal bovine serum (Gibco), 2 mM GlutaMax (Thermo Fisher Scientific), and 1% penicillin-streptomycin (Gibco), at 37 °C and 5% CO_2. Cells were seeded on 24-well glass-bottom plates (Cellvis) or 96-well plates (Cellvis) before transfection. Transfection of HEK293FT and HeLa cells was performed when cells were 40 - 60% confluent with TransIT transfection reagent (Mirus Bio) according to the manufacturer's instructions. Briefly, for a 24-well plate well, 500 ng of plasmid DNA was mixed with 1.5 μl of TransIT reagent in 50 μl opti-MEM (Gibco). After 30-min incubation, the DNA and transfection reagent mix were added to the cell culture medium dropwise. Imaging was then performed 24 hours post-transfection.

U2OS cells (ATCC) were grown and maintained in McCoy's 5A medium (Gibco) supplemented with 10% heat-inactivated fetal bovine serum (Gibco) and 1% penicillin-streptomycin (Gibco), at 37 °C and 5% CO_2. The protocols for seeding and transfection of U2OS cells were the same as those used for HEK293FT cells. For transfection of multiple constructs, plasmids were added to opti-MEM with a total amount of 500 ng and an equal ratio. The plasmid DNA was then fully mixed by vortexing before TransIT transfection reagent was added. Imaging was performed 48 hours post-transfection.

NIH/3T3 cells (ATCC) were grown and maintained in Dulbecco's modified Eagle's medium (DMEM) (Gibco) supplemented with 10% bovine calf serum (Millipore Sigma) at 37 °C with 5% CO_2. NIH/3T3 cells were tested for mycoplasma contamination every 3 months. NIH/3T3 cells were seeded on 24-well glass-bottom plates and transfection was performed when they were 40 - 60% confluent using Lipofectamine 3000 (Thermo Fisher), following the manufacturer's instructions. For transfection of multiple constructs, equal amounts of plasmid constructs were fully mixed in opti-MEM (Gibco) via vortexing before the transfection reagent was added. Imaging was performed 16 to 48 hours post-transfection.

Zebrafish

Procedures at MIT involving animals were in accordance with the National Institutes of Health Guide for the care and use of laboratory animals and approved by the Massachusetts Institute of Technology Animal Care and Use Committee. Zebrafish were raised and bred at 28 °C according to standard methods. Zebrafish larvae were used for experiments on day 5 postfertilization without regard to sex.

METHOD DETAILS

Molecular cloning

Plasmids used in this study were constructed by either restriction cloning or In-Fusion assembly. Sanger sequencing was used to verify DNA sequences. The genes of Dronpa,[20] YFP,[25] and mCherry[31] were amplified from Addgene plasmids 57260, 1816, and

Please cite this article in press as: Qian et al., Temporally multiplexed imaging of dynamic signaling networks in living cells, Cell (2023), https://doi.org/10.1016/j.cell.2023.11.010

55148 respectively. The genes for rsFastLime,[21] rsGreenF,[22] Skylan-NS,[23] rsEGFP2,[22,24] rsTagRFP,[26] rsFusionRed1[27] and GFP enhancer nanobody[22] were synthesized de novo by Integrated DNA Technologies based on the reported sequences. Site-directed mutagenesis libraries were generated using Quikchange site-directed mutagenesis (Agilent). For expression in bacteria, genes were cloned into pBAD-HisD vector. For ubiquitous expression in mammalian cells, genes were cloned into plasmids with one of the three promoters: CMV promoter, EF-1α promoter, CAG promoter. For expression in zebrafish, genes were cloned into the pTol2-10xUAS backbone (for Gal4-dependent expression).[33,34]

All synthetic DNA oligonucleotides used for cloning were purchased from either Integrated DNA Technologies or Quintarabio. PCR amplification was performed using CloneAmp HiFi PCR Premix (Takara Bio). Restriction endonucleases and T4 DNA ligase were purchased from New England BioLabs and used according to the manufacturer's protocols. In-Fusion assembly master mix (Takaro Bio) was used following the manufacturer's instructions for plasmid In-Fusion assembly. Small-scale isolation of plasmid DNA was performed with plasmid mini-prep kits (Takara Bio); large-scale DNA plasmid purification was done by Quintarabio. Plasmids of rScarlet variants were isolated and purified using 96-well plasmid miniprep kits (Bioland Scientific LLC). Stellar Competent cells (Takara Bio) were used for cloning, small-scale DNA plasmid purification, and protein purification; DH5α or NEB Stable Competent cells (New England Biolabs) were used for large-scale DNA plasmid purification.

Screening of reversibly photoswitchable fluorescent proteins

To screen a green photoswitchable fluorescent protein with an off-switching rate between Dronpa and rsFastLime, eight variants carrying mutations at position no. 62 of Skylan were constructed and transiently expressed in HEK293FT cells individually. A 70-frame brief movie (12 s) was then recorded for each variant using an epifluorescence inverted microscope (Eclipse Ti-E, Nikon) equipped with an Orca-Flash4.0 V2 sCMOS camera (Hamamatsu) and a SPECTRA X light engine (Lumencor). NIS-Elements Advanced Research (Nikon) was used for automated microscope and camera control. Cells were imaged with a 40× NA 1.15 water-immersion objective lens (Nikon) at room temperature (excitation: 475/28 nm at 15 mW/mm^2, emission: 525/50 nm). Purple light (390/22 nm at 2 mW/mm^2 for 100 ms) was applied right before taking brief movies. The off-switching traces of each variant were extracted from 8 to 10 cells. The cells were chosen so that they were evenly distributed over the field of views. Skylan62A was the winner of the screening. The off-switching traces of rsGreenF, rsGreenF with the enhancer nanobody, rsEGFP2, and rsEGFP2 with the enhancer nanobody were also obtained using similar imaging setups and analysis (excitation: 475/28 nm at 5 mW/mm^2, emission: 525/50 nm).

For the screening of a red photoswitchable fluorescent protein with a slow off-switching rate, six mutations borrowed from rsCherryRev1.4[29,30] were introduced to mScarlet followed by site-directed saturation at position no.148 and no.162 of mScarlet[28] using the following primer: 5'atgggctggttcgcgNNCaccgagcagttgtaccccgaggacggcgtgctgaagggccttKSCaagatggccctgcgcctg-3'. The plasmids of 196 variants were then amplified, isolated, and expressed individually in HEK293FT cells. Brief movies (70 frames in 12 s) were then recorded (excitation: 555/28 at 9.4 mW/mm^2, emission: 630/75 nm; on-switching: 475/28 nm at 9.6 mW/ mm^2 for 100 ms) for the variants with detectable fluorescence on the same wide-field microscope used for the screening of green photoswitchable fluorescent proteins. The off-switching traces of each tested variant were then extracted from 8 to 10 cells that were evenly distributed over the field of views. The winner of the screening was named rScarlet.

Protein purification and in vitro characterization

To purify each protein sample for characterization, single E. coli colonies expressing each protein were picked and cultured in 2 mL liquid lysogeny broth (LB) medium supplemented with 100 μg/mL ampicillin at 37 °C overnight. This 2-mL culture was then inoculated into a 500 ml liquid LB medium supplemented with 100 μg/mL ampicillin and 0.02% L-arabinose (wt/vol) and cultured at 28 °C for 24 h. After culture, bacteria were harvested by centrifugation. Protein purification was then performed using Capturem His-tagged purification maxiprep kit (Takara bio) following the manufacturer's instructions. Purified proteins were subjected to buffer exchange to 1X TBS (pH = 7.4) with centrifugal concentrators (GE Healthcare Life Sciences).

Absorption, excitation, and emission spectra of purified Skylan62A and rScarlet were measured using a Tecan Spark microplate reader. Extinction coefficients of Skylan62A and rScarlet were determined by first measuring the absorption spectrum of Skylan62A or rScarlet in 1X TBS. The concentration of each protein was then determined by measuring the absorbance of alkaline-denatured protein and assuming ε = 44,000 M^{-1}cm^{-1} at 446 nm.[67] The extinction coefficient (ε) of the protein was calculated by dividing the peak absorbance maximum by the concentration of protein. Proteins were switched to the "on" state with the illumination of purple light before each measurement.

To determine fluorescence quantum yields of Skylan62A and rScarlet, Skylan-NS and mScarlet-I were used as standards respectively. Briefly, the concentration of Skylan62A (or rScarlet) in 1X TBS was adjusted such that absorbance at the excitation wavelength was between 0.1 and 0.2. A series of dilutions of each protein solution and standard, with absorbance values ranging from 0.005 to 0.02, was prepared. The fluorescence spectrum of each dilution of each standard and protein solution was recorded and the total fluorescence intensities were obtained by integration. FPs were switched to their "on" state with the illumination of purple light before each measurement. Absorbance versus integrated fluorescence intensity was plotted for each protein and each standard. Quantum yield (Φ) was calculated from the slopes (S) of each line using the equation: $\Phi_{protein} = \Phi_{standard} \times (S_{protein}/S_{standard})$.

Please cite this article in press as: Qian et al., Temporally multiplexed imaging of dynamic signaling networks in living cells, Cell (2023), https://doi.org/10.1016/j.cell.2023.11.010

Temporal multiplexing of rsFPs in U2OS cells for subcellular labeling

Temporal multiplexing of green rsFPs

rsGreenF-E was fused with an ER-targeting sequence (MLLSVPLLLGLLGLAVA) on the N-terminus and an ER-retention signal sequence (KDEL) on the C-terminus[68]; rsEGFP2-E was fused with histone H2B on the N-terminus; rsFastLime was fused with a mitochondria targeting sequence (MSVLTPLLLRGLTGSARRLPVPRAKIHSL, from Addgene plasmid 57287) on the N-terminus; Skylan62A was fused with Tubulin (from Addgene plasmid 57302) on the C-terminus; Dronpa was fused with α-actinin (from Addgene plasmid 57260) on the N-terminus, YFP was fused with LAMP1 on the N-terminus (Addgene plasmid 1816)[65] (the choice of FP for each subcellular-targeting sequence was random, however, we recommend using slower-switching FPs to label fine or sparse subcellular structures due to the larger number of photons they produce in a given brief movie). Six more constructs were built by adding a FLAG-tag (DYKDDDK) to the C-terminus of each FP in the previous six constructs.

The six constructs with FLAG-tag were expressed in U2OS cells individually. In parallel, one of the FLAG-tagged constructs was coexpressed with the other five non-FLAG constructs in U2OS cells. Cells with the expression of subcellular compartment-targeted FPs were then fixed with 4% paraformaldehyde (PFA) 48 hours after transfection followed by two washes with 1X PBS and one wash with 1X Phosphate-Buffered Saline (PBS) containing 100 mM glycine at room temperature. Cells were permeabilized with 0.1% Triton X-100 for 10 minutes and then blocked with MAXBlock Blocking medium (Active Motif) for 15 min, followed by three washes for 5 minutes each at room temperature in 1X PBS. Next, samples were incubated with rabbit anti-FLAG antibody (Invitrogen) in MAXStain Staining medium (Active Motif) for 1 hour at room temperature followed by three washes for 5 minutes each at room temperature in 1X PBS. Then, samples were incubated with Alexa647-labeled goat-anti-rabbit antibody (Abcam) in MAXStain Staining medium (Active Motif) for 1 hour at room temperature followed by three washes for 5 minutes each at room temperature in 1X PBS. Samples were then stored in 1X PBS and imaged on a Nikon Eclipse Ti inverted microscope equipped with a spinning disk confocal (CSU-W1), a 40×, 1.15 NA water-immersion objective, and a 5.5 Zyla camera (Andor), controlled by NIS-Elements AR software.

For the imaging of the cells with only one FLAG-tagged construct expressed, two snapshot images were taken from the green channel (exposure time 50ms, excitation: 488nm, emission: 525/30 nm) and far-red channel (exposure time 50ms, excitation: 637nm, emission: 700/50nm) for each field-of-view (FOV). A colocalization test was then run between the two images from the same FOV to get a Pearson's correlation value (cell masks were used for the test). For the imaging of the cells with 6 constructs expressed (one FLAG-tagged construct plus five constructs without FLAG tag), a 70-frame brief movie (3.8 s) and a snapshot image were taken from the green (exposure time 50ms, excitation: 488nm at 40 mW/mm^2, emission: 525/30 nm) and far-red channel, respectively for each FOV. Six unmixed images were obtained via signal unmixing of each brief movie. The unmixed image from the FLAG-tagged construct was then colocalized with the image taken from the same FOV via far-red channel to get a Pearson's correlation value. Purple light (405 nm at 9.7 mW/mm^2) was applied for 50 ms before brief movies were taken.

For the imaging of live U2OS cells co-expressing rsGreenF-E-ER, Skylan62A-Tubulin, and YFP-LAMP, the same plasmid constructs and spinning disk confocal microscope as in the above were used. 405 nm laser light (9.7 mW/mm^2) from the blue channel was on for 50 ms, and then the channel was switched to the green channel to take a 20-frame brief movie (exposure time 20 ms, excitation: 488nm at 55 mW/mm^2, emission: 525/30 nm); the channel was then switched back to the blue channel to repeat the aforementioned imaging process. The acquisition time for each brief movie was 0.5 seconds, and the interval between two brief movies was 5 seconds. Ten brief movies were taken in total.

Temporal multiplexing of red FPs

rsTagRFP was fused with histone H2B (same as the tag fused to rsEGFP2-E in the previous experiment) on the N-terminus, rsFusionRed was fused to Human Vimentin Sequence (from Addgene plasmid 57306) on the C-terminus. rScarlet was fused with α-actinin (same as the tag fused to Dronpa in the previous experiment) on the N-terminus. mCherry was fused with a mitochondrial targeting sequence (same as the tag fused to rsFastLime in the previous experiment) on the N-terminus. (the choice of FP for each subcellular-targeting sequence was random, however, we recommend using slower-switching FPs to label fine or sparse subcellular structures due to the larger number of photons they produce in a given brief movie).Four more constructs were built by adding a FLAG-tag (DYKDDDK) to the C-terminus of each FP in the aforementioned four constructs.

The protocols for cell transfection, fixation, and immunostaining were the same as those for green FPs. Imaging of red FPs was also performed on the same microscope as the imaging of the green FPs. For the imaging of the cells with only one FLAG-tagged construct expressed, two snapshot images were taken from the red channel (exposure time 100ms, excitation: 561nm, emission: 579/34 nm) and far-red channel (exposure time 50ms, excitation: 637nm, emission: 700/50nm) for each FOV. A colocalization test was then run between the two images from the same FOV to get a Pearson's correlation value. For the imaging of the cells with 4 constructs expressed (one FLAG-tagged construct plus three constructs without FLAG tag), a 70-frame brief movie (8.6 s) and a snapshot image were taken from the red (excitation: 561nm at 50 mW/mm^2, emission: 579/34 nm) and far-red channel, respectively for each FOV. Four unmixed images were obtained via signal unmixing of each brief movie. The unmixed image from the FLAG-tagged construct was then co-localized with the image taken from the same FOV via far-red channel to get a Pearson's correlation value. Cyan light (488 nm at 40 mW/mm^2) was applied for 50 ms before brief movies were taken.

For the imaging of live U2OS cells co-expressing rsGreenF-E-ER, Skylan62A-Tubulin, YFP-LAMP, H2B-rsTagRFP, rsFusionRed1-vimentin, and mitochondria-targeted mCherry, the same plasmid constructs and spinning disk confocal microscope as above were used. Two 20-frame brief movies were taken from the green channel (exposure time 20 ms, excitation: 488nm at 55 mW/mm^2, emission: 525/30 nm) and the red channel (exposure time 100 ms, excitation: 561nm at 50 mW/mm^2, emission: 579/34 nm), respectively,

Please cite this article in press as: Qian et al., Temporally multiplexed imaging of dynamic signaling networks in living cells, Cell (2023), https://doi.org/10.1016/j.cell.2023.11.010

for each FOV. The acquisition times for brief movies taken from the green and red channel were 0.5 seconds and 2.5 seconds, respectively.

Crosstalk measurements

For the crosstalk measurements of green FPs, seeded NIH3T3 cells were transfected with pcDuex2-rsGreenF-E, pcDuex2-rsEGFP2-E, pcDuex2-rsFastLime, pcDuex2-Skylan62A, pcDuex2-Dronpa, and pcDuex2-YFP separately in 6 different wells of 24-well plates. Three hours after transfection, the growth medium with transfection reagents of each well was aspirated and the cells were then washed with 1x PBS three times followed by trypsin treatment (0.05% trypsin-EDTA (Gibco)) for 2 mins. The detached cells from each well were then suspended and collected before being fully mixed with the cells from the other 5 wells. Mixed cells were then seeded back to 24-well plates (note that the transfection efficiency for the protocol described here is lower than the standard protocol mentioned previously). 16-24 hours after re-seeding, imaging was performed on a Nikon Eclipse Ti inverted microscope equipped with a confocal spinning disk (CSU-W1), a 20×, 0.75 NA air objective, and a 5.5 Zyla camera (Andor), controlled by NIS-Elements AR software. For each FOV, a 70-frame brief movie (12 s) was taken (exposure time, 50ms, excitation: 488nm at 10 mW/mm^2, emission: 525/30 nm, on-switch:405 nm at 2.5 mW/mm^2 for 100ms) and 6 unmixed images were obtained via signal unmixing. Since each transfected cell only expressed one FP, the crosstalks of the expressed FP to other FPs were calculated as the percentages of the fluorescence of other FP channels in that cell to the fluorescence of the expressed FP channel in the same cell.

The crosstalk measurements of red FPs were similar to that of green FPs except that only four plasmids (pcDuex2-rsTagRFP, pcDuex2-rsFusionRed1, pcDuex2-rScarlet, pcDuex2-mCherry) were used and brief movies (12 s) were taken using the red channel (exposure time: 100ms, excitation: 561 nm at 12.5 mW/mm^2, emission: 579/34 nm, on-switch: 488 nm at 10 mW/mm^2 for 100ms).

TMI simulation

For simulations of temporal multiplexing, we used a pre-acquired fluorescent image (the image was taken on a Nikon epifluorescence inverted microscope with a 20×, 0.75 NA air objective; image size: 1024 × 1024) of NIH/3T3 cells expressing Dronpa to generate brief movies for both green FPs and red FPs. Segmentation was first applied to the fluorescent image to convert Dronpa-expressing cells to cell-shaped masks. Then, the normalized traces of six green FPs (or four red FPs) were scaled, each with a random ratio (the sum of the ratios equals 1) to create a hybrid trace for each mask (different masks contained different ratios of the six FPs, same masks contained the same ratios of the six FPs). Next, the values of hybrid traces (ranging from 0 to 1) at each time point (20 to 100 time-points in total) were used to multiply the fluorescence value of each pixel within the cell-shaped masks to generate a brief movie (the fluorescence of the non-masking area was assigned as 0) with a frame number of either 70 (Figures 3F, 4F, S7, and S13) or 20-100 with an interval of 20 (Figure S27). Poisson noises were then calculated according to the fluorescence intensity at each pixel ($Poisson\ noise = \sqrt{F * Conversion\ factor * B^2}$; F, fluorescence intensity in each pixel; conversion factor of the camera we used, 0.46; B, pixel binning) and then applied back to each pixel of the brief movie (Poisson noise and Gaussian noise are the two major sources of noises in fluorescence microscopy. In the simulated experiments, the Poisson noise ranged from 15 - 300 electrons for each pixel whereas the Gaussian noise was only 1.6 electrons for each pixel according to the manufacturer of Orca-Flash4.0 V2 sCMOS camera (Hamamatsu). Thus, we only included Poisson noise, for simplicity). In the meantime, six ground truth images (or four ground truth images for red FPs) were generated by multiplying the randomly assigned ratio of each FP by the fluorescence of the pre-acquired fluorescence image at each pixel within the cell-shaped masks. The fluorescence of the FPs in the non-masking area was assigned as 0. The code for TMI simulation is available on https://github.com/qiany09/Temporally-Multiplexed-Imaging.

Zebrafish Imaging

DNA plasmids encoding rsTagRFP, rsFusionRed1, and rScarlet under the control of the 10x UAS promoter were mixed with a ratio of 2:2:1 and co-injected with Tol2 transposase mRNA into embryos of the pan-neuronal expressing Gal4 line, Tg (elavl3:GAL4-VP16).[69] Briefly, Tol2 transposase mRNA, synthesized using pCR2FA as a template[70] (mMESSAGE mMACHINE SP6 Transcription Kit, Thermo Fisher), and DNA was diluted to a final concentration of 25 ng/μl in 0.4 mM KCl solution containing 0.05% phenol red solution (Millipore Sigma) to monitor the injection quality. The mixture was kept on ice to minimize the degradation of mRNA during the injection. The mixture was injected into embryos at 1-cell stage.[71] Larvae were screened for red fluorescence in the brain and spinal cord at day 3 post fertilization (animals were used without regard to sex) and subsequently imaged on day 5 post fertilization. To image zebrafish larvae, larvae were immobilized in 1.5% ultra-low-melting agarose (Millipore Sigma) prepared in E3 medium and paralyzed with 0.2 mg/ml pancuronium bromide (Millipore Sigma). Imaging was performed on a Nikon Eclipse Ti inverted microscope equipped with a confocal spinning disk (CSU-W1), a 40×, 1.15 NA water-immersion objective, and a 5.5 Zyla camera (Andor), controlled by NIS-Elements AR software. A 60-frame brief movie (8.6 s) was taken for each FOV (exposure time 100ms, excitation: 561nm at 50 mW/mm^2, emission: 579/34 nm, on-switch: 488 nm at 40 mW/mm^2 for 50ms). References traces for this experiment were extracted from HEK293FT cells expressing individual FPs.

Imaging of cell cycle phases and kinase activities in NIH3T3 cells

FUCCI4 constructs were gifts from Michael Z Lin (Addgene no. 83841-83942).[35] Single-color FUCCI4 was built by replacing Clover, mKO2, mMaroon1, and mTurquoise2 with rsGreenFast-E, Dronpa, Skylan62A, and YFP respectively. 16-24 hours after transfection, NIH/3T3 cells were imaged on an epifluorescence inverted microscope (Eclipse Ti-E, Nikon) equipped with a 20×, 0.75 NA air objective, Perfect Focus System, an Orca-Flash4.0 V2 sCMOS camera (Hamamatsu), and a SPECTRA X light engine (Lumencor). Cells

Please cite this article in press as: Qian et al., Temporally multiplexed imaging of dynamic signaling networks in living cells, Cell (2023), https://doi.org/10.1016/j.cell.2023.11.010

were placed in a stage-top incubator with a controlled environment at 37°C and 5% humidified CO_2 (Live Cell Instrument), and brief movies (60 frames in 15 s, excitation light was on during the whole 15s) were acquired every 30 min. Excitation: 475/28 nm at 9.6 mW/mm^2, emission: 525/50 nm, exposure time: 50 ms, on switching: 390/22 nm at 1.2 mW/mm^2 for 100ms.

The constructs of JNK KTR-rsGreenFast-E, P38 KTR-Dronpa, ERK KTR-rsFastLime were built based on the original KTRs constructs JNK KTR-Clover (Addgene plasmid 59151), P38 KTR-mCerulean3 (Addgene plasmid 59155), ERK KTR-Clover (Addgene plasmid 59150), all gift of Markus W. Covert.[37] The newly developed three KTRs were then used along with PKA KTR-Clover (Addgene plasmid 59151) and H2B-TagBFP2 to report the activities of all four kinases. H2B-TagBFP2 was used as a nucleus marker. NIH/3T3 cells were imaged on the same microscope and incubator system as the imaging of cell cycle phases. Cell culture media were changed to imaging media (MEM (Gibco) without phenol red with 1% FBS (Gibco)) prior to imaging. Brief movies were acquired with the excitation of 475/28 nm at 3.2 mW/mm^2, and emission of 525/50 nm (60 frames in 15 s, exposure time: 50 ms, excitation light was on during the whole 15s). Images of H2B-TagBFP2 (excitation: 390/22 nm at 1.2 mW/mm^2; emission: 447/60 nm, exposure time: 100ms) were acquired right before recording brief movies to switch rsFPs to the "on"-state. Images and brief movies were acquired every 2 min. 50 μM Forskolin (Millipore Sigma), and 20 ng/ml basic fibroblast growth factor2 (bFGF2, R&D System) were used to activate kinase activities. Control experiments without addition of forskolin or bFGF2 were also performed under the same imaging conditions.

ROS measurements

NIH/3T3 cells were transfected with JNK KTR-rsGreenFast-E, P38 KTR-Dronpa, ERK KTR-rsFastLime, PKA KTR-Clover, and H2B-TagBFP2. Before imaging, cells were incubated with the CellROX Orange dye (Invitrogen) at a final concentration of 5 μM for 30 min at 37 °C in darkness and then washed three times with PBS before adding 500 μl MEM (without phenol red) supplemented with 1% FBS. Orange fluorescence (excitation: 555/28 at 9.4 mW/mm^2, emission: 630/75 nm; exposure time: 200ms) was imaged every 2 min under 3 conditions: darkness (for 1 hour), illumination of 390/22 nm at 1.2mW/mm^2 for 50 ms followed by 475/28 nm at 3.2 mW/mm^2 for 15 s every 2 min (for 1 hour), and illumination of 475/28 nm at 0.96 mW/mm^2 for 50ms at 10 Hz (for 16 minutes). To measure ROS level under the imaging condition used for TMI-based FUCCI4, NIH/3T3 cells with the loading of CellRox orange dye (5 μM) were imaged every 30 min for 12 hours under the following two conditions: darkness and illumination of 390/22 nm at 1.2mW/mm^2 for 50 ms followed by 475/28 nm at 9.6 mW/mm^2 for 15 s.

Combined temporal multiplexing and spectral multiplexing

Simultaneous imaging of cell cycle phases and activity of cyclin-dependant kinases

To increase the number of genes co-expressed within single cells, the four genes encoding FUCCI4 were cloned into a single plasmid as the following: CMV-rsGreenFast-Geminin$_{1\text{-}110}$-P2A-Dronpa-cdt$_{30\text{-}120}$-IRES-H1-Skylan62A-P2A-YFP-SLBP$_{18\text{-}126}$. NIH3T3 cells were then transfected with the aforementioned plasmid, plasmid EF1α-DHB-TagBFP2,[47] and plasmid EF1α-mCherry-CDK4KTR.[48] Imaging was performed 16-24 hours post-transfection on the same epifluorescence inverted microscope and incubation system as described previously. Blue channel (excitation: 390/22 nm at 1.2 mW/mm^2; emission: 447/60 nm, exposure time: 100ms), green channel (60 frames in 15 s, excitation light (475/28 nm at 9.6 mW/mm^2) was on during the whole 15 s, emission: 525/50 nm; exposure time: 50ms) and red channel (excitation: 555/28 nm at 9.4 mW/mm^2, emission: 630/75 nm; exposure time: 100ms) were used together for imaging of 6 signals. Purple light illumination used in the blue channel for excitation also served as the "on" trigger for green rsFPs. Images and brief movies were acquired every 30 min for 24-48 hours without stimulation.

Simultaneous imaging of seven cell activities within single cells

The genes of the single-color KTRs were cloned into the following plasmid: CAG-JNKKTR-rsGreenF-E-P2A-ERKKTR-rsFastLime-IRES-PKAKTR-Clover-P2A-P38KTR-Dropna. The aforementioned plasmid was then used with plasmid CAG-NIR-GECO2G,[51] plasmid CMV-Pink Flamindo,[52] and plasmid CMV-BlueCKAR[2] for imaging 7 signals within individual NIH/3T3 cells. Imaging conditions for blue channel, green channel, and red channel were the same as those used in the imaging of cell cycle phases and CDK activities. An extra channel (excitation: 637/12 nm at 9 mW/mm^2; emission: 664LP, exposure time: 100ms) was used for imaging NIR-GECO2G. Images and brief movies were acquired every 2 min. 50 μM forskolin (Millipore Sigma) and 100 ng/ml phorbol 12-myristate 13-acetate (PMA) (Millipore Sigma) were used to stimulate cells.

Signal unmixing and image analysis

Signal unmixing of temporal multiplexed imaging

Reference traces of FPs used for signal unmixing were collected right before or after each imaging experiment. Each reference trace was an averaged result from 10 to 30 cells of 2 to 3 brief movies from one cell culture batch. Traces from each cell were normalized to the maximum value before averaging. Cells were selected so they were evenly distributed on the fields-of-views. For signal unmixing of temporal multiplexing imaging, the recorded trace at each pixel was first normalized to the maximum value and then unmixed into a linear combination of the reference traces of fluorophores using least squares regression. Next, the resultant ratios (ranging from 0 to 1) of fluorophores at each pixel were multiplied by the fluorescence value of the first frame of the brief movie at this very pixel to generate unmixed images. The code for signal unmixing is available at https://github.com/qiany09/Temporally-Multiplexed-Imaging.

Please cite this article in press as: Qian et al., Temporally multiplexed imaging of dynamic signaling networks in living cells, Cell (2023), https://doi.org/10.1016/j.cell.2023.11.010

Brief movies were processed in Fiji as follows before being subjected to signal unmixing using custom Matlab code (or before being used for extracting reference traces): images were down-sampled from size 2048x2048 to size 1024x1024 or size 512x512 (to decrease computing time) followed by background subtraction.

Quantification of KTRs

Kinase activities reported by KTRs including the CDK2 reporter and CDK4/6 reporter were quantified following the methods described previously.[48] Briefly, to calculate cytoplasmic intensity to nuclear intensity, a nucleus and a five-pixel-wide cytoplasm ring were segmented for each cell via nucleus-targeted fluorescent proteins. Nucleus segmentation and cell tracking were performed in Fiji using StarDist[66] and trackmate, respectively. Cytoplasmic rings were segmented by using a custom macro in Fiji. Median intensity extracted from each ROI was used to calculate ratios. The ratios reflect kinase activity. CDK4/6 activity was then corrected by deducting 0.35-fold CDK2 activity, as before.[48] $(\Delta R/R_0)$max in Figures 4E–4L is defined as the average of the maximum value and the two values before and after the time point of maximum value for a given kinase trace. $(\Delta R/R_0)$tail is defined as the average of the values of the last three time points of a given kinase trace. $(\Delta R/R_0)$max under forskolin stimulation in Figures 5G and 5H is defined as the average of the maximum value (in the first 44 min before the addition of PMA) and the two values before and after the time point of maximum value for a given kinase trace.

Analysis of CDK2 and CDK4/6 activity traces (Figures 5C and 5D)

CDK traces of each cell were first divided into sub-traces of different cell cycle phases. Each sub-trace of a complete cell cycle phase was then evenly split into three parts. A value was obtained by averaging all the data points in one part, thus yielding 3 values representing CDK activity at early, middle and late stages of each cell cycle phase, for a given cell.

All images in the manuscript were processed and analyzed using Fiji and NIS-Elements. Traces and graphs were generated using GraphPad Prism 8 or Origin9.0.

QUANTIFICATION AND STATISTICAL ANALYSIS

All statistical analysis was performed using the built-in statistical analysis tools in GraphPad Prism 8 or Origin9.0. Details of our statistical analysis can be found in the figure legends and Table S3.

CellPress
OPEN ACCESS

Supplemental figures

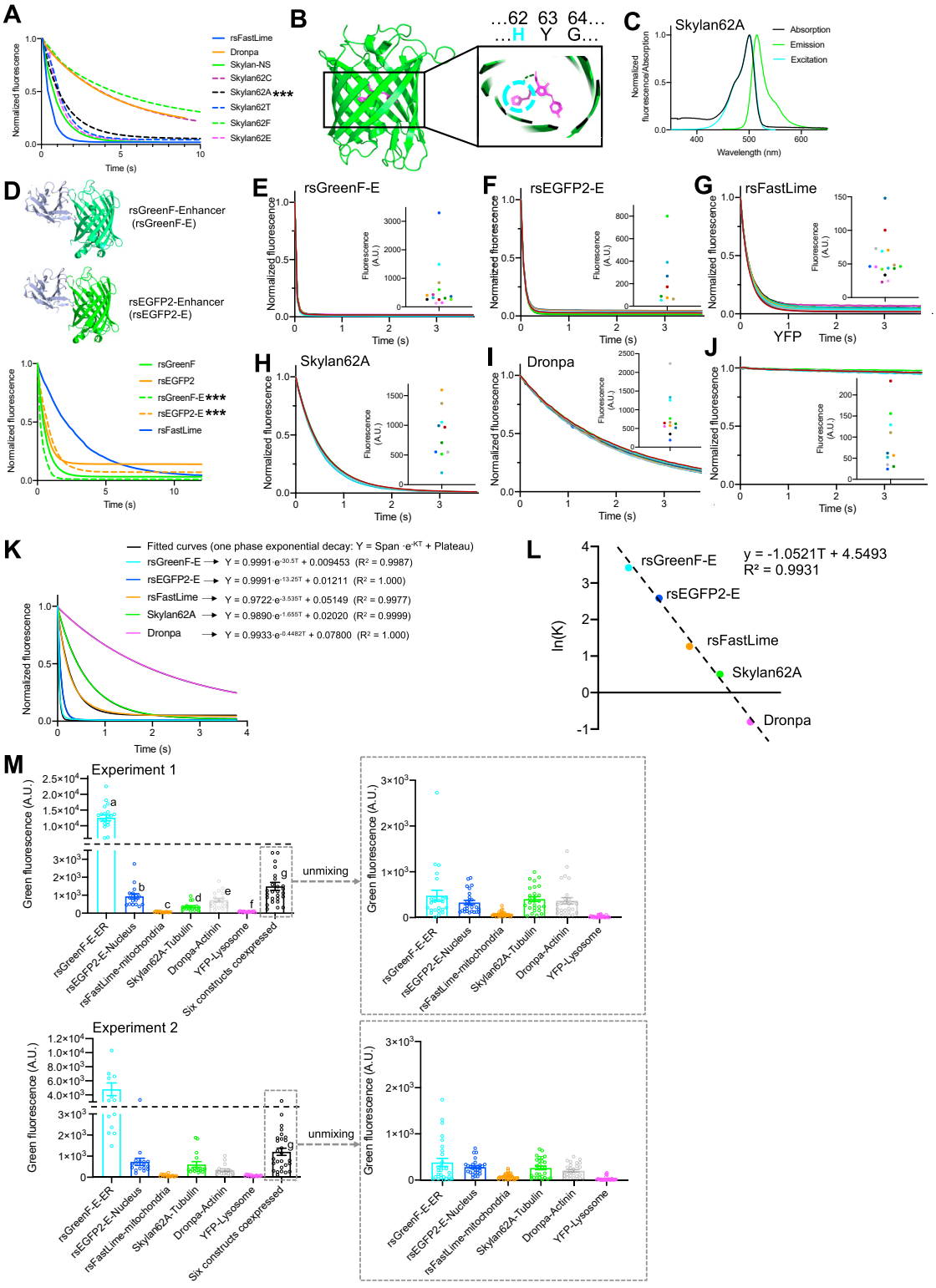

(legend on next page)

Figure S1. Development of green rsFPs for TMI and TMI characterization with green FPs, related to Figure 2

(A) Off-switching traces of a series of Skylan mutants obtained in HEK293FT cells; rsFastLime and Dronpa were also tested under the same conditions for reference. Averaged values are shown, n = 8–12 cells from one culture. Excitation: 475/28 nm at 15 mW/mm^2 (wide-field microscopy). Skylan62A (indicated by triple stars) was the winner of the screening.

(B) Crystal structure of mEosFP (PDB: 3S05). The chromophore (highlighted in magenta) of mEosFP is formed by the tripeptide HYG (histidine-tyrosine-glycine). Inspired by the engineering of photoswitchable Skylan-NS from mEos3.1, which was achieved by mutating His62 (highlighted by dashed cyan circle) to Leu, a photoswitchable FP, Skylan62A (Skylan-NS-Leu62Ala), was developed from Skylan-NS by screening the off-switching rates of a library carrying mutations at position 62 of Skylan-NS. The off-switching rate of Skylan62A is in between that of Dronpa and rsFastLime, which makes Skylan62A a good candidate for TMI with rsFastLime and Dronpa.

(C) Absorption (black), excitation (cyan), and emission (green) spectra of Skylan62A.

(D) Top, structure of rsGreenF-Enhancer (rsGreenF-E) and rsEGFP2-Enhancer (rsEGFP2-E). Bottom, off-switching traces of rsGreenF and rsEGFP2 with and without enhancer recorded in HEK293FT cells. rsFastLime was also tested under the same conditions for reference. Averaged values are shown, n = 6–10 cells from one culture. Excitation: 475/28 nm at 5 mW/mm^2 (wide-field microscopy). The addition of a nanobody enhancer increases the photoswitching kinetics of rsGreenF and decreases the photoswitching rate of rsEGFP2. rsGreenF-E and rsEGFP2-E (indicated by triple stars) were then chosen for TMI.

(E–J) Off-switching rates of green rsFPs are independent of protein concentrations. Off-switching traces of rsGreenF-E (E), rsEGFP2-E (F), rsFastLime (G), Skylan62A (H), Dronpa (I), and YFP (J) in U2OS cells. The FPs were fused to the same subcellular targeting sequences as in Figure 2C. Individual traces from 10 to 15 cells (from 2 or 3 brief movies from 1 cell culture) are shown for each FP and normalized to peak. Illumination: 488 nm at 40 mW/mm^2 (confocal microscopy). Imaging conditions are the same as those in Figure 2B. Inset, fluorescence intensity (used to estimate protein concentration) of individual cells; same color represents the same cell within each panel (e.g., blue trace in A and the blue dot in the inset of A represent the fluorescence trace and protein concentration of the same cell). a.u., arbitrary units.

(K) Off-switching traces (same as in Figure 2B) of rsGreenF-E (cyan), rsEGFP2-E (blue), rsFastLime (orange), Skylan62A (green), Dronpa (magenta), as well as their exponential fit curves (black, plotted under the empirical traces; most are hard to see because the overlap is so good). The fitted exponential decay equations ($Y = \text{span} \cdot e^{-KT} + \text{plateau}$, Y represents normalized fluorescence, T represents time, K is time constant) of the traces and their R^2 (the coefficient of determination) are shown in the upper right.

(L) The natural logarithms of the time constants (ln(K)) of the green rsFPs used in TMI are evenly distributed. When we use 1–5 to represent the x axis values of the rsFPs (from fastest photoswitching to lowest photoswitching) and the natural logarithms of the time constants of the corresponding rsFPs to represent their y axis values, the data points of the 5 rsFPs are well defined by a linear equation (as shown on the upper right corner of the panel).

(M) Comparisons of protein concentration between cells co-expressing six green FPs with subcellular targeting sequences and cells expressing single green FPs with subcellular targeting sequences. Bar plots of green fluorescence intensity (excitation: 488 nm, emission: 525/30 nm [confocal microscopy]), a.u., arbitrary unit, fluorescence intensity is used as a proxy for protein concentration, with each circle representing the fluorescence averaged across one cell. In each experiment, the same amount of plasmid DNA was used for cell transfection. To express only one construct in cells, 500 ng of plasmid DNA was used for transfecting each well of cells seeded on 24-well plates; to co-express all six constructs in the same cells, a total of 500 ng plasmid DNA (~83 ng for each construct) was used for each well of cells seeded on 24-well plates (cells were plated with similar confluency across different wells and plates). The fluorescence of the cells expressing one or more constructs was then imaged, and their averaged fluorescence intensity was calculated as a to g. a to f represent the averaged fluorescence intensity of each group of cells expressing the single construct indicated. (a + b + c + d + e + f)/6 was then used to roughly represent the expected average fluorescence if a cell expressed each of the six constructs at 1/6 the level of when they expressed each construct alone; g, the fluorescence intensity across the cell when all 6 constructs were actually expressed. g was then compared to (a + b + c + d + e + f)/6. The coefficient, 0.6 for experiment 1 and 1.1 for experiment 2, indicates how far off the actual intensity of expressing all 6 constructs was from this divided-by-six calculation. Bar plots of mean ± SEM are used with individual values plotted as dots (each dot is one cell). Data from two cell culture batches are shown (denoted as experiment 1 and 2, respectively; n = 20, 17, 14, 17, 18, 17, and 27 cells for rsGreenF-E-ER, rsEGFP2-E-Nucleus, rsFastLime-mitochondria, Skylan62A-Tubulin, Dronpa-Actinin, YFP-Lysosome, and the six constructs co-expressed, respectively, in experiment 1; n = 14, 17, 15, 16, 16, 15, and 27 cells for rsGreenF-E-ER, rsEGFP2-E-Nucleus, rsFastLime-mitochondria, Skylan62A-Tubulin, Dronpa-Actinin, YFP-Lysosome, and the six constructs co-expressed, respectively, in experiment 2).

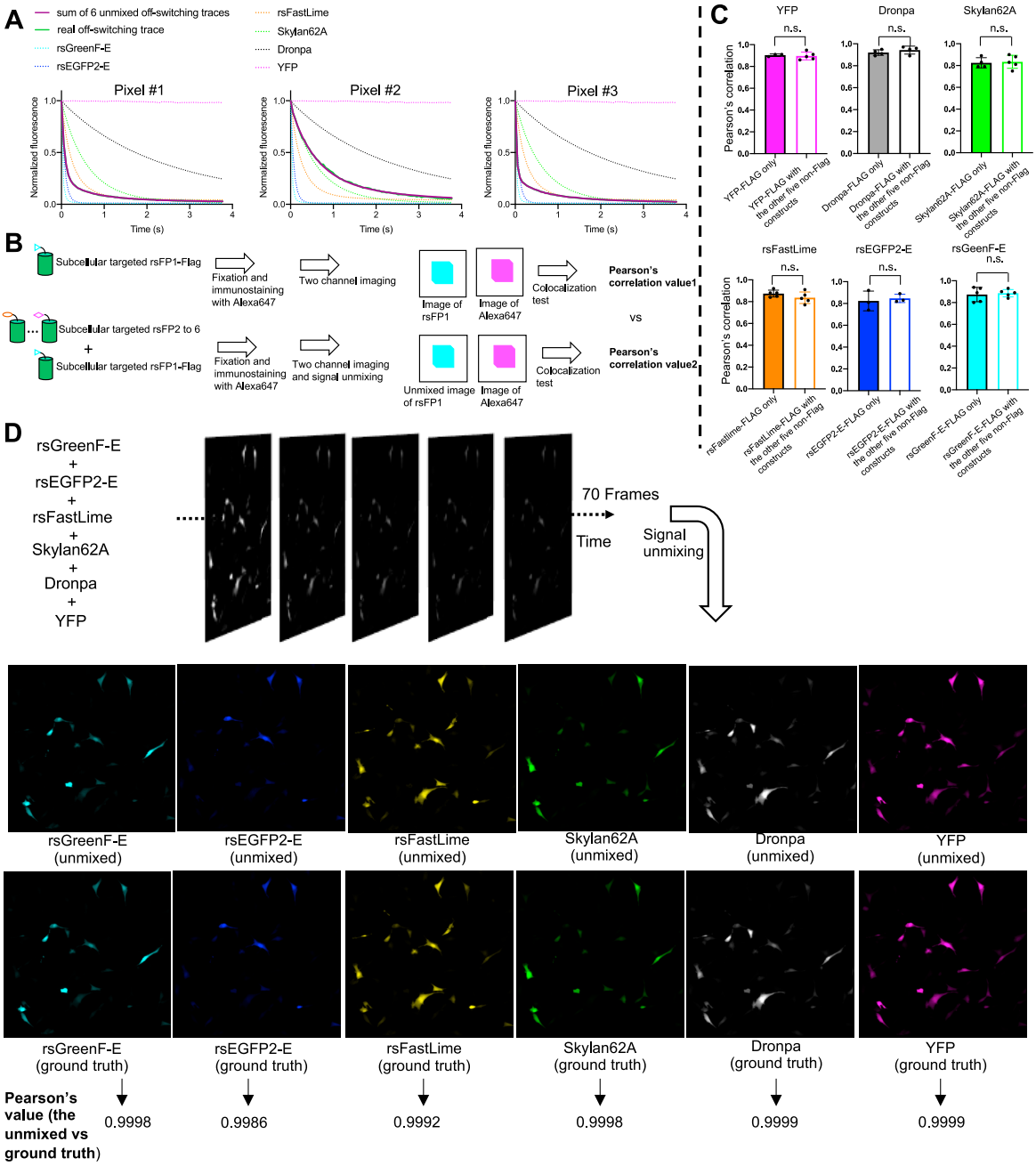

Figure S2. Further characterization of TMI with green FPs, related to Figure 2

(A) Three pixels randomly chosen from the brief movie in Figure 2C are shown. Reference traces used for signal unmixing are shown as dashed lines. The real trace is plotted under the trace representing the sum-of-6 unmixed off-switching traces and thus is not easily visible, because the two traces are so similar.

(B) Experimental design for evaluating TMI using green FPs. A FLAG tag was added to each of the six subcellularly targeted constructs. In the first experiment, as shown on the upper panel, each FLAG-tagged construct was expressed individually in U2OS cells. 48 h post transfection, cells were fixed and immuno-stained with Alexa647 dye. Two snapshot images were taken from green channel (excitation: 488 nm, emission: 525/30 nm) and far-red channel (excitation: 637 nm, emission: 700/50 nm) followed by co-localization test and calculation of Pearson's correlation values. In the second experiment, as shown on the bottom panel, one FLAG-tagged construct was co-expressed with other five constructs without a FLAG tag in U2OS cells, 48 h post transfection; a 70-frame brief movie was taken from the green channel, and a snapshot image was taken from the far-red channel. After signal unmixing, six images were obtained from the green channel. The unmixed image of the FLAG-tagged construct was then co-localized with the image obtained from far-red channel followed by calculation of another set of Pearson's correlation values. The two sets of Pearson's correlation values were then compared for each FP. A spinning disk confocal microscope was used for this experiment.

(legend continued on next page)

(C) Bar plots of Pearson's correlation values of each FP obtained in (B). n = 3–6 images from two cell culture batches. Data are shown as mean ± SD with individual values plotted as dots. Unpaired t test was run between two sets of Pearson's correlation values for each FP; n.s., no significance..
(D) Simulation of TMI of six green FPs. A 70-frame brief movie was generated using a pre-acquired fluorescence image of NIH/3T3 cells and the off-switching traces in Figure 2B. The fluorescence components of the six FPs in each cell were randomly assigned. Different cells thus had different fluorescence combinations of the six FPs. Top, simulated brief movie showing cells that express six green rsFPs. Bottom, after signal unmixing, six images were obtained for the FPs. The images were then compared with ground-truth images. Pearson's correlation values between unmixed images and ground-truth images are shown. Detailed value comparisons are shown in Figure 2F.

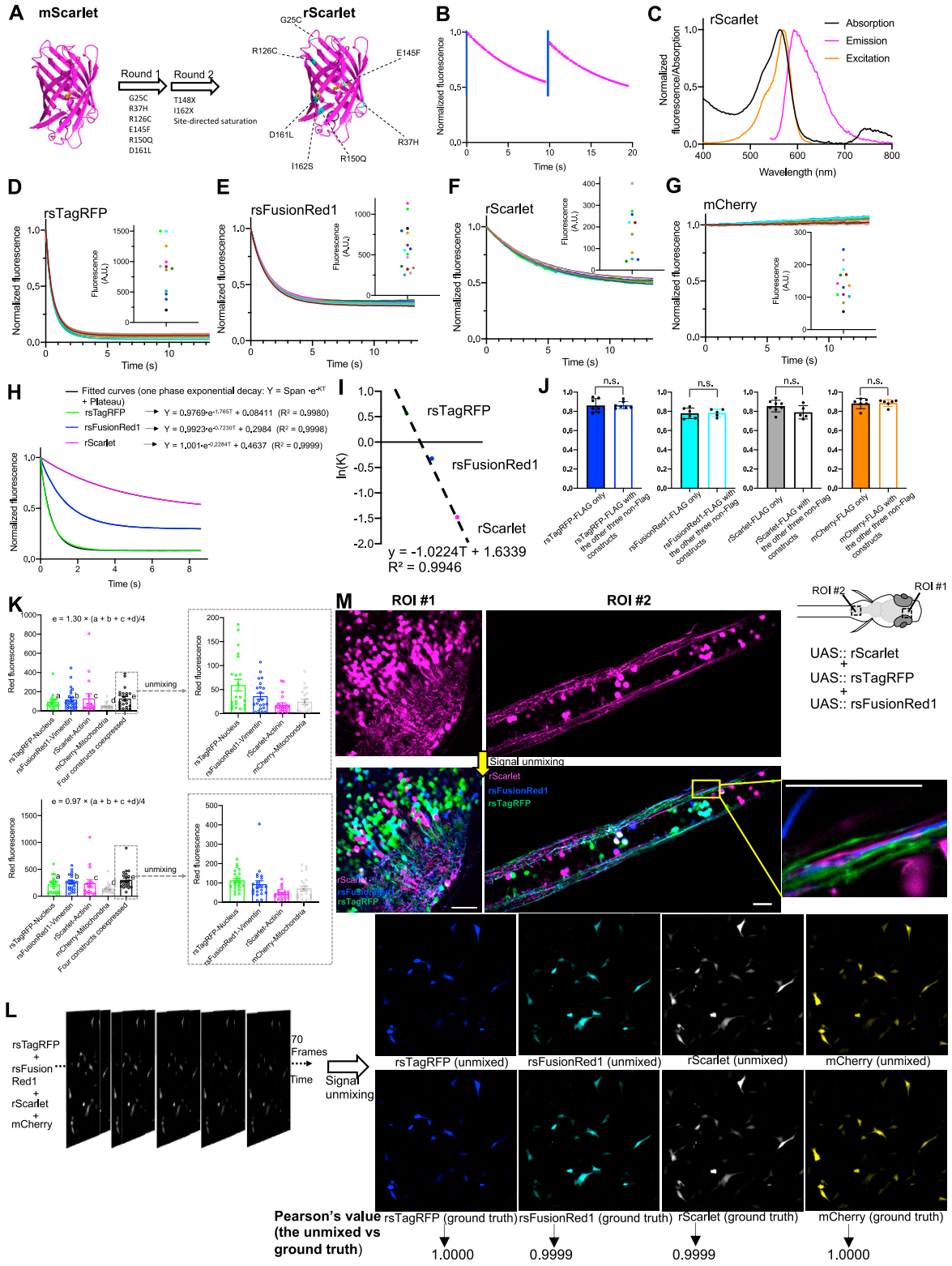

Figure S3. Development of a red rsFP for TMI and TMI characterization with red FPs, related to Figure 3

(A) Schematic illustration of the engineering of rScarlet from mScarlet. Left, crystal structure of mScarlet; the chromophore is shown in orange. Two rounds of evolution were performed before photoswitchable rScarlet was selected. rScarlet accumulated seven mutations compared to mScarlet, which is highlighted in

(legend continued on next page)

the crystal structure on the right. The mutations from round 1 are highlighted in cyan, and the mutation (I162S) from round 2 is highlighted in yellow (the amino acid at site no. 148 didn't change during the second-round evolution).
(B) Photoswitching traces of rScarlet in HEK293FT cells, n = 3 cells from one culture. Data are shown as mean ± SD. Excitation: 555/28 nm at 9.4 mW/mm^2, on-switching: 475/28 nm at 9.6 mW/mm^2 for 100 ms (blue bar). Wide-field microscopy was performed for this experiment.
(C) Absorption (black), excitation (orange), and emission (magenta) spectra of rScarlet.
(D–G) Off-switching rates of red rsFPs are independent of protein concentrations. Off-switching traces of rsTagRFP (D), rsFusionRed1 (E), rScarlet (F), and mCherry (G) in U2OS cells. The FPs were fused to the same subcellular targeting sequences as in Figure 3C. Individual traces from 10 to 15 cells from 1 cell culture are shown for each FP and normalized to peak. Excitation: 561 nm at 50 mW/mm^2 (confocal microscopy). Imaging conditions are the same as those in Figure 3B. Inset, fluorescence intensity (used to estimate protein concentration) of individual cells; same color represents the same cell within each panel. a.u., arbitrary unit.
(H) Off-switching traces (same as in Figure 3B) of rsTagRFP (green), rsFusionRed1 (blue), rScarlet (magenta), and their fitting curves (black, under the data traces, and thus not always visible). The fitted exponential decay equations of the traces and their R^2 (the coefficient of determination) are shown in the upper right.
(I) The natural logarithms of the time constants of the red rsFPs used in TMI are equally spaced. When we use 1–3 (from fastest photoswitching to lowest photoswitching) to represent the x axis values of the rsFPs, and use the natural logarithms of time constants of the rsFPs to represent their y axis values, the data points of the 3 red rsFPs are well defined by a linear equation (as shown on the bottom of the panel).
(J) The same experiments as in Figure S2B were run for the four red FPs used in TMI, and two sets of Pearson's correlation values were obtained for each red FP. Bar plots of mean with SD are used, with individual values plotted as dots; n = 5–6 images from two cell culture batches. Unpaired t tests were run between two sets of Pearson's correlation values for each FP; n.s., no significance..
(K) Comparisons of protein concentration between cells co-expressing four red FPs with subcellular targeting sequences and cells expressing single red FPs with subcellular targeting sequences. Bar plots of red fluorescence intensity (excitation: 561 nm, emission: 579/34 nm (confocal microscopy), a.u., arbitrary unit, fluorescence intensity is used as a proxy for protein concentration), with each circle representing the fluorescence averaged across one cell. In each experiment, the same amount of plasmid DNA was used for cell transfection. To express only one construct in cells, 500 ng of plasmid DNA was used for each well of cells seeded on 24-well plates; to co-express all four constructs in the same cells, a total of 500 ng plasmid DNA (~125 ng for each construct) was used for each well of cells seeded on 24-well plates (cells were plated with similar confluency across different wells and plates). The fluorescence of the cells expressing one or more constructs was then imaged, and their averaged fluorescence intensity was calculated as a to e; a to d represent the averaged fluorescence intensity of each group of cells expressing the single construct indicated. (a + b + c + d)/4 was then used to roughly represent the expected average fluorescence of a cell expressing each of the four constructs at 1/4 the level that they would have, expressing each construct alone; e, the intensity across the cell when all 4 constructs are expressed, is then compared to the expected average fluorescence (a + b + c + d)/4.The calculated coefficient, 1.3 for experiment 1 and 0.97 for experiment 2, indicates how far off the actual intensity of expressing all 4 constructs was from this divided-by-4 calculation. Bar plots of mean ± SEM are used with individual values plotted as dots. Data from two cell culture batches are shown (denoted as experiment 1 and 2, respectively; n = 16, 27, 17, 18, and 22 cells for rsTagRFP-Nucleus, rsFusionRed1-Vimentin, rScarlet-Actinin, mCherry-Mitochondria, and the four constructs co-expressed, respectively, in experiment 1; n = 18, 22, 18, 18, and 22 cells for rsTagRFP-Nucleus, rsFusionRed1-Vimentin, rScarlet-Actinin, mCherry-Mitochondria, and the four constructs co-expressed, respectively, in experiment 2).
(L) Simulation of TMI of four red FPs. A 70-frame brief movie was generated using a pre-acquired fluorescence image of NIH/3T3 cells (same image and methods as used in Figure S2D) and the off-switching traces in Figure 3B. Left, simulated brief movie showing cells that express four red FPs. Right, after signal unmixing, four images were obtained for the FPs. The images were then compared with ground-truth images. Pearson's correlation values between unmixed images and ground-truth images are shown. Detailed value comparisons are shown in Figure 3F.
(M) More images of single-color brainbow in zebrafish. Top, representative raw fluorescent images (out of 20 images taken from 3 animals) of zebrafish larvae in spinal cord and forebrain (dorsal view). Bottom, brainbow-like images showing the same area in the images on the top. TMI-based brainbow is able to distinguish nearby neurites from different neurons (bottom left). All scale bars, 20 μm.

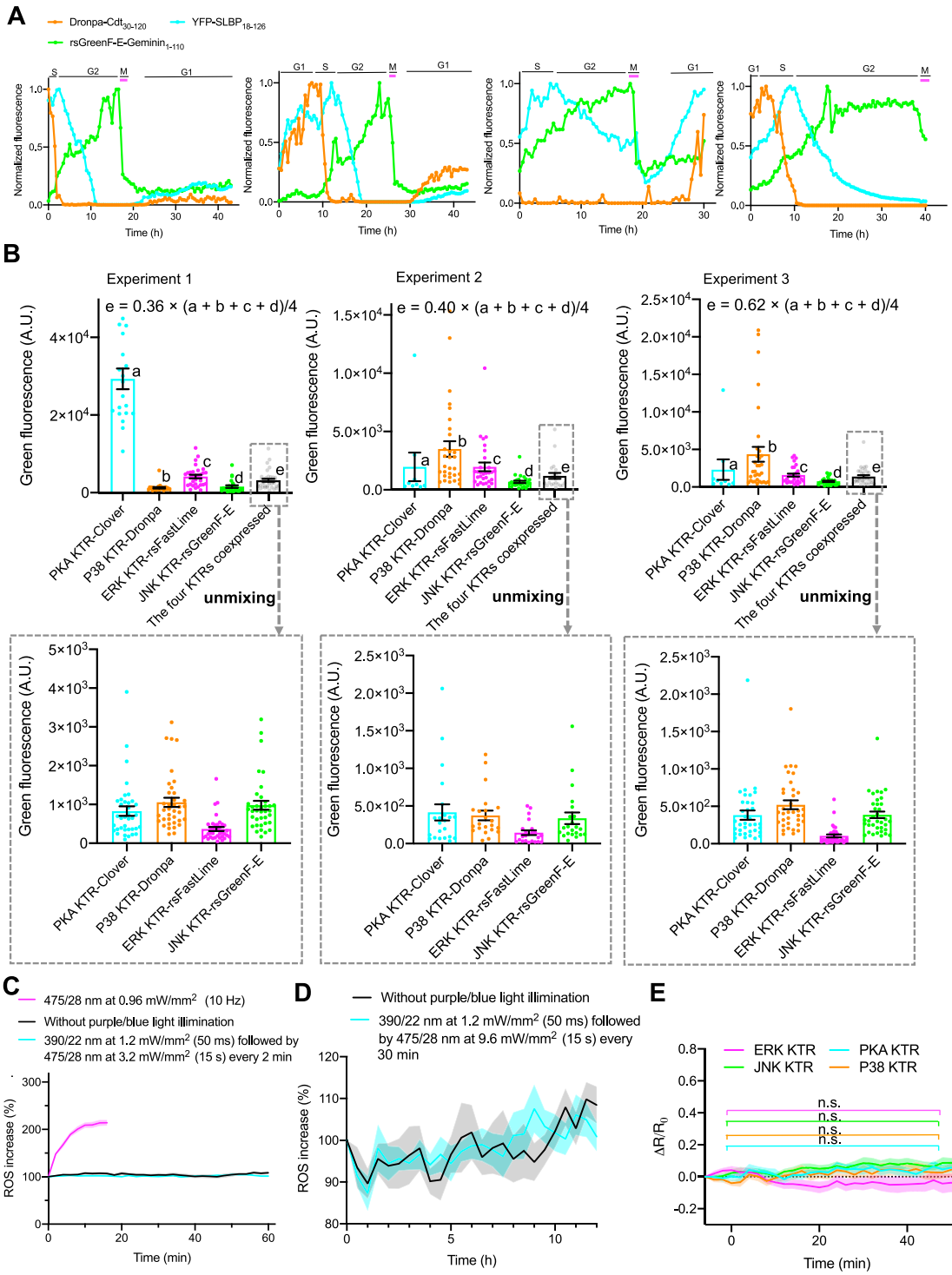

Figure S4. Characterization of TMI for imaging many dynamic signals within single cells, related to Figure 4

(A) Additional fluorescence traces of Dronpa-Cdt1$_{30–120}$ (orange), rsGreenF-E-Geminin$_{1–110}$ (green), and YFP-SLBP$_{18–126}$ (cyan) during cell divisions, tracing one arbitrary daughter cell from each mother cell when the cell divides. Fluorescence was normalized to maximum value. Magenta bars indicate observation of chromosome condensation. Cell-cycle phases were assigned based on the principles in Figure 4A.

(B) Comparisons of protein concentration between cells co-expressing four KTRs and cells expressing single KTRs. Similar experiments and analysis to those in Figures S1M and S3K were performed. Bar plots of green fluorescence intensity (excitation: 475/28 nm, emission: 525/50 nm) (wide-field microscopy), a.u., arbitrary unit, fluorescence intensity is used as a proxy for protein concentration), with each circle representing the fluorescence averaged across one cell. The

(legend continued on next page)

averaged fluorescence intensity of cells expressing only one KTR was denoted as a to d; (a + b + c + d)/4 was then used to roughly represent the expected average fluorescence of a cell expressing each of the four KTRs at 1/4 the level that they would have, expressing each KTR alone; e, the fluorescence intensity across the cell when all 4 KTRs are expressed is then compared to the expected average fluorescence (a + b + c + d)/4, calculated as if a cell expressing all 4 KTRs were to express each at 1/4 the level that they would when expressing each KTR alone. The calculated coefficients, 0.36, 0.40, and 0.62 for experiments 1, 2, and 3, respectively, indicate how far off the actual intensity of expressing all 4 constructs was from this divided-by-4 calculation. Bar plots of mean ± SEM are used with individual values plotted as dots. Data from three cell cultures are shown (denoted as experiment 1, 2, and 3, respectively; n = 20, 27, 31, 25, and 37 cells for PKA KTR-Clover, P38 KTR-Dronpa, ERK KTR-rsFastLime, JNK KTR-rsGreenF-E, and the four KTRs co-expressed, respectively, in experiment 1; n = 9, 30, 30, 27, and 22 cells for PKA KTR-Clover, P38 KTR-Dronpa, ERK KTR-rsFastLime, JNK KTR-rsGreenF-E, and the four KTRs co-expressed, respectively, in experiment 2; n = 9, 33, 30, 28, and 36 cells for PKA KTR-Clover, P38 KTR-Dronpa, ERK KTR-rsFastLime, JNK KTR-rsGreenF-E, and the four KTRs co-expressed, respectively, in experiment 3).

(C) Changes in relative ROS concentration (normalized to that before illumination) of NIH/3T3 cells (with the co-expression of all four KTRs and H2B-TagBFP2) over time under darkness (black, n = 18 cells [from 1 cell culture]), the condition for simultaneous imaging of 4 KTRs (390/22 nm at 1.2 mW/mm^2 for 50 ms followed by 475/28 nm at 3.2 mW/mm^2 for 15 s every 2 min, cyan, n = 25 cells [from two cell cultures]), and illumination of 0.96 mW/mm^2 at 475/28 nm for 50 ms at 10 Hz (magenta, n = 16 cells [from two cell cultures]). Data are shown as mean ± SEM.

(D) Changes in relative ROS concentration (normalized to that before illumination) of NIH/3T3 cells over 12 h under darkness (black, n = 9 cells [from two cell culture batches]), and the condition for imaging of TMI-based single-color FUCCI4 (390/22 nm at 1.2 mW/mm^2 for 50 ms followed by 475/28 nm at 9.6 mW/mm^2 for 15 s every 30 min, cyan, n = 10 cells [from two cell cultures]). Data are shown as mean ± SEM.

(E) Averaged traces of four kinase activities recorded from NIH/3T3 cells under purple/blue illumination (390/22 nm at 1.2 mW/mm^2 for 50 ms followed by 475/28 nm at 3.2 mW/mm^2 for 15 s every 2 min) without drug stimulation; n = 12 cells from two cell cultures. Data are shown as mean ± SEM. Wilcoxon rank-sum tests were run between the values from t = −6 to t = 0 min and t = 48 to t = 54 min for all KTRs. Throughout the figure: n.s., no significance.

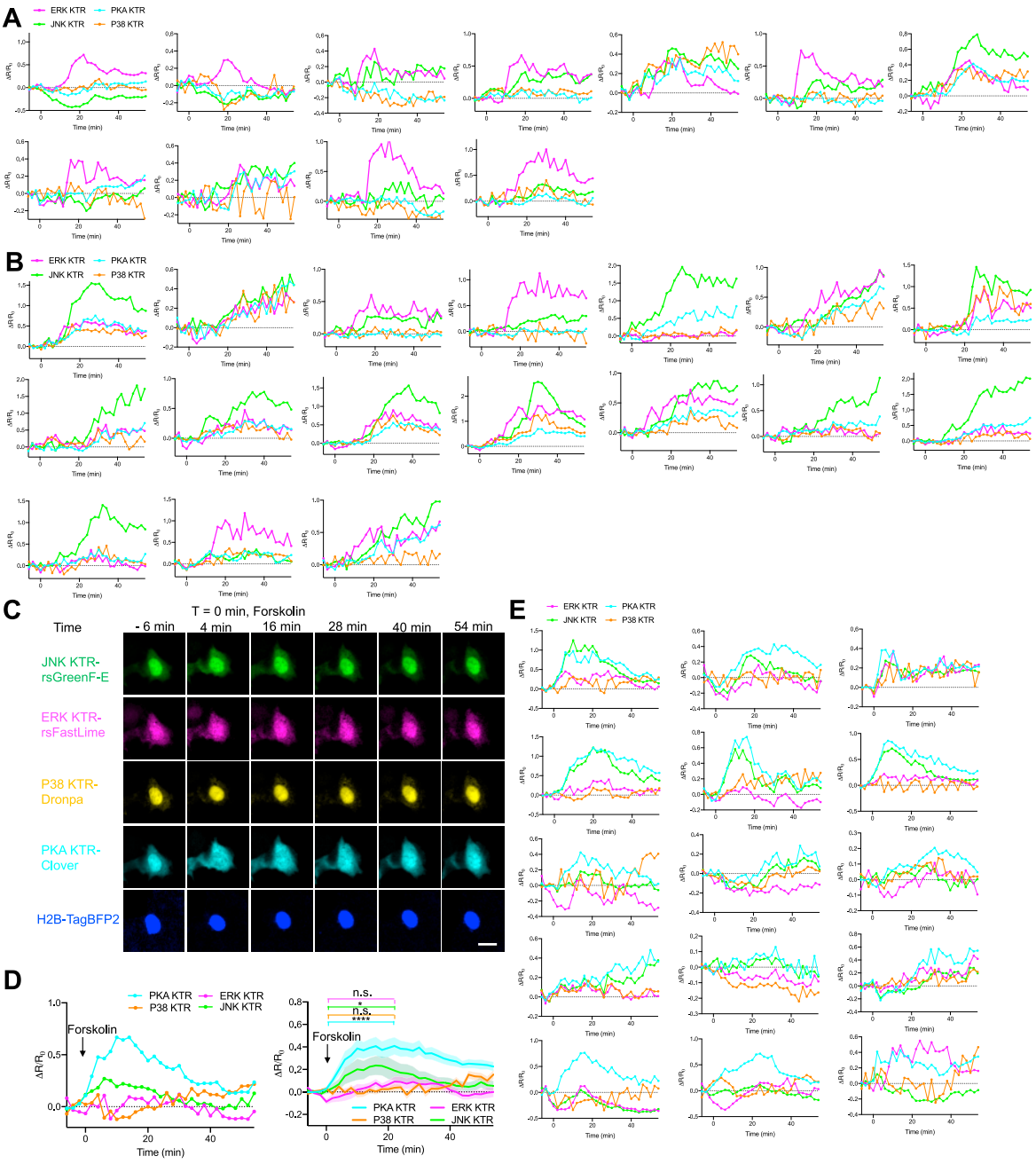

Figure S5. Additional data for temporally multiplexed imaging of many dynamic signals in single cells, related to Figure 4

(A and B) Activity traces of ERK KTR-rsFastLime, JNK KTR-rsGreenF-E, P38 KTR-Dronpa, and PKA KTR-Clover from individual cells upon stimulation with 20 ng/mL bFGF2, added at t = 0 min. The averaged traces of those in (A) (type 1 cells) are shown in Figure 4H, left. The averaged traces of those in (B) (type 2 cells) are shown in Figure 4H, right. The averaged traces of all cells are shown in Figure 4G.

(C–E) Responses of ERK KTR-rsFastLime, JNK KTR-rsGreenF-E, P38 KTR-Dronpa, and PKA KTR-Clover after treatment with forskolin. (C) Representative NIH/3T3 cell expressing all four KTR sensors and H2B-TagBFP2 was stimulated with 50 μM forskolin and imaged at the indicated time points. Forskolin was added at t = 0 min. Scale bar, 20 μm. (D) Left, fluorescence traces of ERK KTR, JNK KTR, P38 KTR, and PKA KTR from the cell in (A). Right, averaged traces of four kinase activities recorded from NIH/3T3 cells, with stimulation of 50 μM forskolin at t = 0 min; n = 16 cells (from two culture batches). Data are shown as mean ± SEM. Wilcoxon rank-sum tests were run between the averaged values from t = −6 to t = 0 min and t = 18 to t = 24 min for all KTRs, *$p < 0.05$, ****$p < 0.0001$, n.s., no significance. (E) Additional kinase activity traces from individual cells. Forskolin was added at t = 0 min. Throughout the figure, R: cytoplasmic intensity to nuclear intensity ratio, change in fluorescence of the sensors is plotted as $\Delta R/R_0$ (R_0 was the averaged value from t = −6 to t= −4 min).

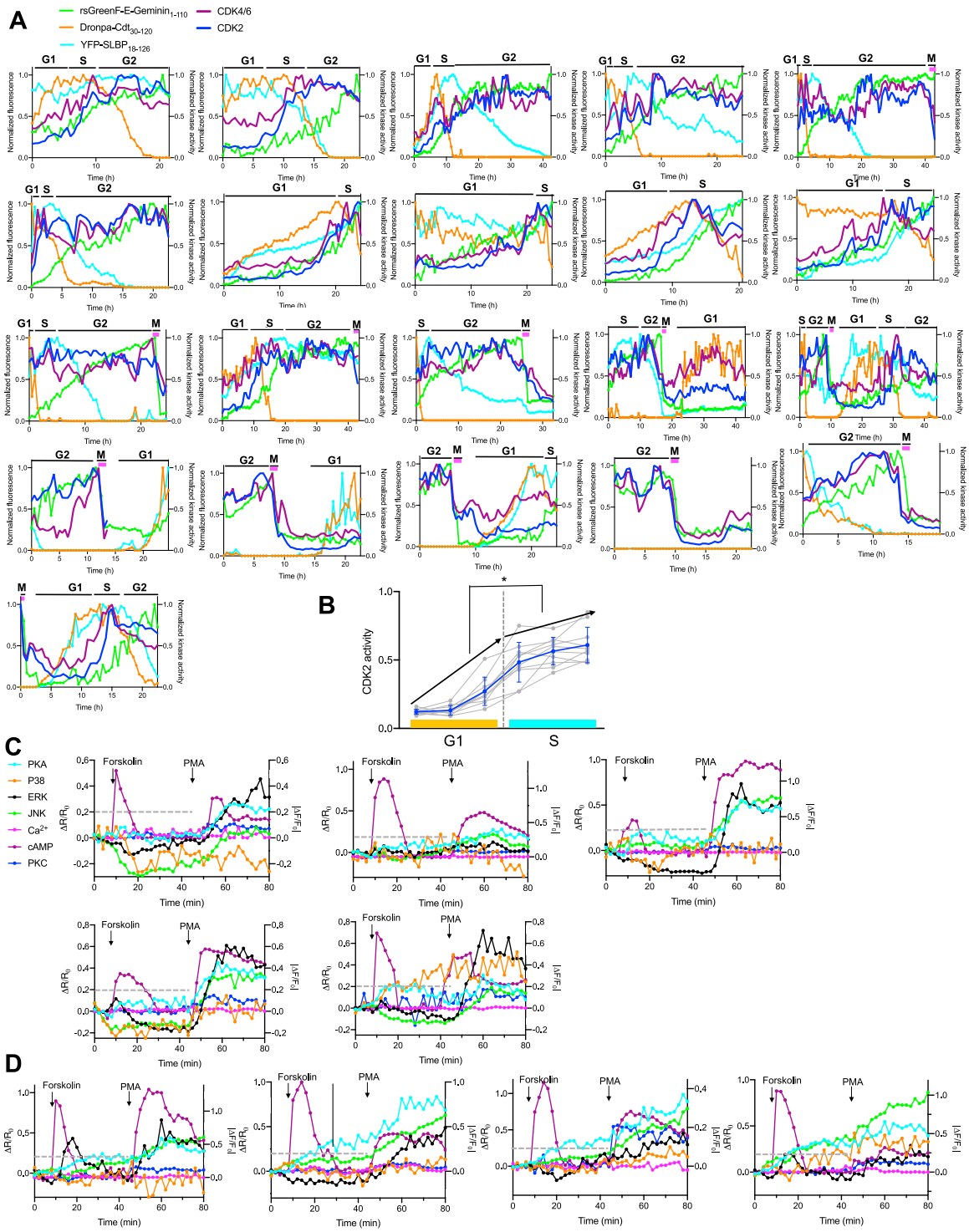

Figure S6. Additional data for combined temporally and spectrally multiplexed imaging, related to Figure 5

(A) Additional traces of four fluorescence signals from FUCCI4 and two CDK signals from corresponding reporters over cell divisions. NIH/3T3 cells were imaged every 30 min without stimulation. Fluorescence signals of Dronpa-Cdt1$_{30–120}$ (orange), rsGreenF-E-Geminin$_{1–110}$ (green), YFP-SLBP$_{18–126}$ (cyan), CDK2 reporter (blue), and CDK4/6 reporter (magenta) were calculated and shown in the same ways as described in Figure 5B.

(B) Comparison of CDK2 activity throughout G1 and S phase. Data are shown as mean ± SD (blue) with all individual values plotted (gray), n = 10 cells from 5 cell culture batches. Wilcoxon rank-sum test was run between the difference in CDK2 activity between the end and beginning of G1 and the difference in CDK2 activity between the end and beginning of S phase, *$p < 0.05$.

(legend continued on next page)

(C and D) Activity traces of P38 (orange), PKA (cyan), ERK (black), JNK (green), Ca^{2+} (magenta), cAMP (purple), and PKC (blue) from single cells with low PKA activity (C, $(\Delta R/R_0)$max under forskolin stimulation <0.2) and high PKA activity (D, $(\Delta R/R_0)$max under forskolin stimulation $\geq$0.2). The classification threshold for low vs. high PKA activity ($\Delta R/R_0$ = 0.2) is shown as a gray dashed line in each plot.

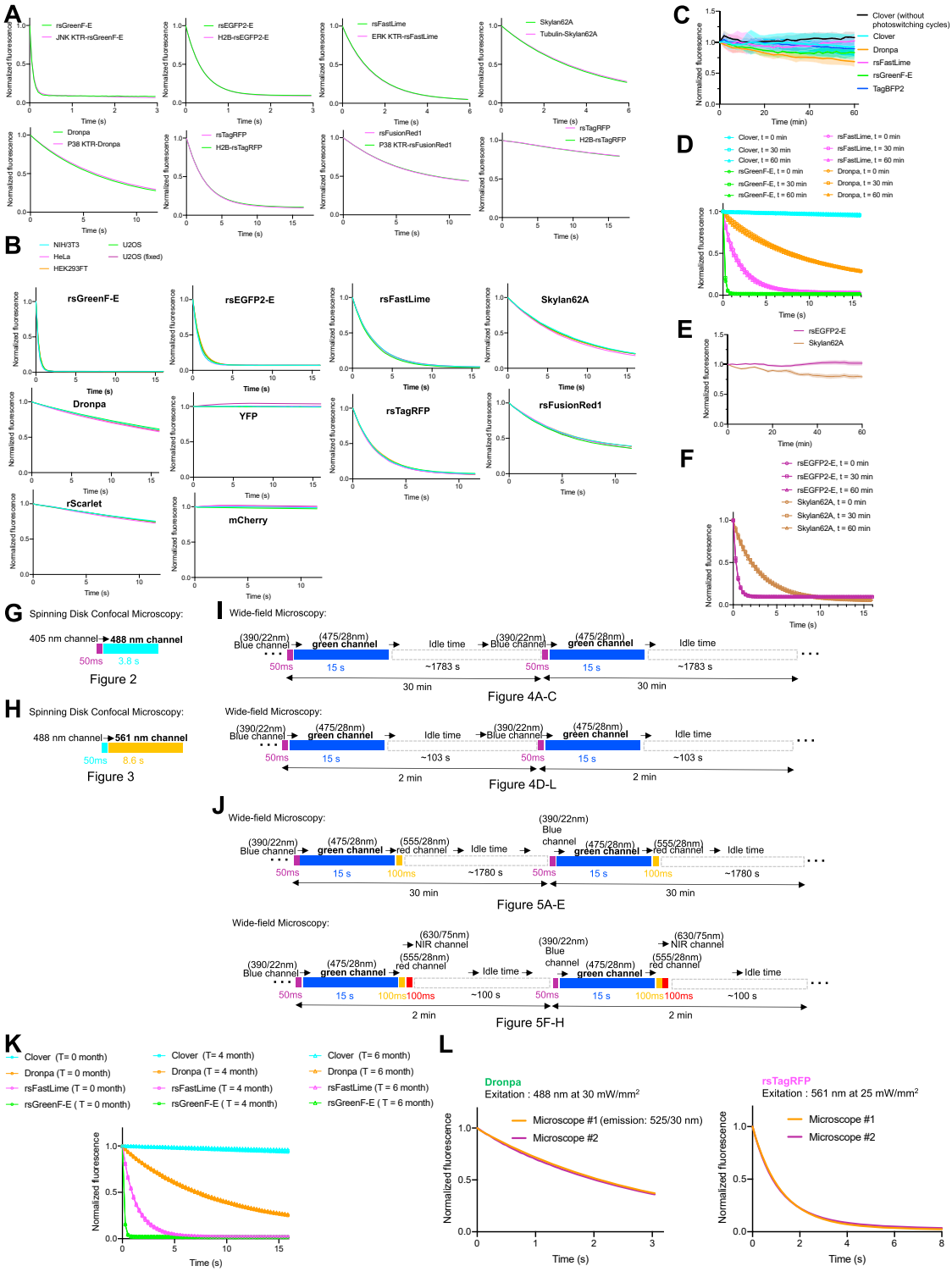

Figure S7. Further characterization and practical consideration of TMI, related to Figure 6

(A) Off-switching traces of rsGreenF-E and JNK KTR-rsGreenF-E, rsEGFP2 and H2B-rsEGFP2, rsFastLime and ERK KTR-rsFastLime, Skylan62A and tubulin-Skylan62A, Dronpa and P38 KTR-Dronpa, rsTagRFP and H2B-rsTagRFP, rsFusionRed1 and P38 KTR-rsFusionRed1, and rScarlet and actinin-rScarlet. Illumination: 475/28 nm at 9.6 mW/mm^2 for the first four pairs, 475/28 nm at 0.96 mW/mm^2 for Dronpa and P38 KTR-Dronpa, and 555/28 at 9.4 mW/mm^2 for the last three pairs; mean values are shown, n = 8–14 cells (from 2 brief movies from 1 cell culture). Wide-field microscopy was performed for this experiment.

(legend continued on next page)

(B) Off-switching kinetics of green rsFPs (including non-switching YFP) and red rsFPs (including non-switching mCherry) were measured in NIH/3T3 cells (cyan), HeLa cells (magenta), HEK293FT cells (orange), U2OS cells (green), and fixed U2OS cells (purple) with a wide-field microscope. Illumination for green FPs: 475/28 nm at 3.2 mW/mm^2; illumination for red FPs: 555/28 at 9.4 mW/mm^2; mean values are shown, n = 10–16 cells (from 3 brief movies from 1 cell culture).
(C–F) Photobleaching profiles of green FPs used in TMI (experiments were performed on a wide-field microscope).
(C) Photobleaching curves of the FPs (Clover, Dronpa, rsFastLime, rsGreenF-E, and TagBFP2) used in TMI for imaging of kinase activity when illuminated by 390/22 nm at 1.2 mW/mm^2 for 50 ms followed by 475/28 nm at 9.6 mW/mm^2 (9.6 mW/mm^2 was only used for this photobleaching test; for measuring kinase activity, 3.2 mW/mm^2 was used throughout the rest of this paper) for 15 s (every 2 min for 1 h); n = 18–23 cells (from 2 or 3 cell cultures, each). Clover was also tested in a separate experiment without taking brief movies (only one snapshot image was taken every 2 min; exposure time, 50 ms; excitation: 475/28 nm at 9.6 mW/mm^2), serving as a reference for conventional imaging; n = 7 cells (from one culture). Solid lines represent mean value, shaded areas represent SD.
(D) Off-switching traces of Clover, Dronpa, rsFastLime, and rsGreenF-E at t = 0, 30, and 60 min during 1-h long imaging sessions under the same imaging conditions as in (C) (for Clover, we did not repeat the snapshot experiment); mean values are shown, n = 10–16 cells (from two cell cultures, each).
(E) Photobleaching curves of rsEGFP2-E and Skylan62A (the two rsFPs that were not used for imaging of kinase activity in this study) under the same imaging conditions as described in (C). Data are show as mean ± SD, n = 15 cells (from one cell culture, each).
(F) Off-switching traces of rsEGFP2-E and rsGreenF-E at t = 0, 30, and 60 min during 1-h-long imaging sessions under the same imaging condition as in (C) and (E); mean values are shown, n = 10 cells (from 1 cell culture, each).
(G–J) Image acquisition flowcharts for experiments in Figures 2, 3, 4, and 5. Optical channels used to take brief movies are in bold. Excitation wavelengths of each channel are shown in the figure. NIR, near-infrared. Note that in (I) and (J), signals from different channels were imaged sequentially, thus the exact acquisition time point for the signals from different channels is slightly different.
(K) Off-switching kinetics of rsGreenF-E (green), rsFastLime (magenta), Dronpa (orange), and Clover (cyan) in 3 different experiments spanning 6 months (T = 0, 4, and 6 months); mean values are shown, n = 16–20 cells (from 3 brief movies from 1 cell culture each). Illumination (wide-field microscopy): 475/28 nm at 9.6 mW/mm^2.
(L) Off-switching kinetics of Dronpa and rsTagRFP acquired under two different spinning disk confocal microscopes (microscope #1: Nikon CSU-W1, microscope #2: Nikon CSU-W1-SoRa) with the same laser illumination (488 nm at 30 mW/mm^2 for Dronpa, 561 nm at 25 mW/mm^2 for rsTagRFP); mean values are shown, n = 8–15 cells (from 2 brief movies from 1 cell culture).